Geophys. J. Int. (2001) **145,** 246–264

Variation in the crustal structure across central Iceland

Zhijun Du[1] and G. R. Foulger[2]

[1] *Institute of Theoretical Geophysics, University of Cambridge, Downing Street, Cambridge,* CB2 3EQ, *UK. E-mail: Zhijun.Du@itg.cam.ac.uk*
[2] *Department of Geological Sciences, University of Durham, South Road, Durham,* DH1 3LE, *UK. E-mail: G.R.Foulger@durham.ac.uk*

Accepted 2000 November 6. Received 2000 November 1; in original form 2000 March 28

SUMMARY

We determine the crustal structures beneath 12 broad-band seismic stations deployed in a swath across central Iceland along and around the ICEMELT explosion seismic profile by combining teleseismic receiver functions, surface wave dispersion curves and the waveforms of a large, local event in Iceland. By using teleseisms that approach from different backazimuths, we study lateral structural variability out of the line of the ICEMELT profile. Beneath Tertiary areas, the thickness of the upper crust, as defined by the 6.5 km s^{-1} velocity horizon, is $\sim$8 km and the depth to the base of the lower crust, as defined by the 7.2 km s^{-1} velocity horizon, is $\sim$29–32 km. Beneath the currently active rift zone the upper crust thins to $\sim$6.0 km and the depth to the base of the lower crust increases to $\sim$35–40 km. A substantial low-velocity zone underlies the Middle Volcanic Zone in the lower crust, which may indicate anomalously high geothermal gradients there. This suggests that the large-scale thermal centre of the hotspot may be more westerly than northwest Vatnajokull, where it is generally assumed to lie. Simplified description of the results notwithstanding, there is substantial variability in the overall style of crustal structure throughout Iceland, and a clear, tripartite division into upper and lower crusts and a sharp Moho is poorly supported by many of our results. The nature, distinctiveness and continuity of the Moho is variable and in many areas the crust–mantle transition is a zone with enhanced velocity gradients several kilometres thick.

Key words: crustal structure, Iceland, receiver functions, surface waves, velocity gradients, waveforms.

INTRODUCTION

Central Iceland is a geological complex comprising several contrasting tectonic elements (Fig. 1). Prior to $\sim$5 Ma the accretionary plate boundary extended from Langjokull north through the Skagi peninsula to join with the Kolbeinsey ridge to the north, but it subsequently migrated east and currently forms the Northern Volcanic Zone (NVZ). The Skagi peninsula is thus an extinct rift. The area between the Skagi Peninsula and the currently active NVZ forms a geologically distinct Tertiary block 7–12 Myr old, the Trollaskagi block (Saemundsson *et al.* 1980). South of this block lies the Middle Volcanic Zone (MVZ), a remote and little-studied area dominated by a massive, caldera volcano capped by the Hofsjokull icecap. South of Hofsjokull lies the Eastern Volcanic Zone (EVZ), the most northerly part of which is the highest elevated and most volcanically productive part of Iceland and capped by the northwest part of the Vatnajokull icecap. The EVZ is thought to be a southwestward-propagating rift to which accretionary activity is currently being transferred from the dwindling Western Volcanic Zone (WVZ) (Saemundsson 1979). It is bordered on its southeast side by the Snaefell Flank Zone. The currently active rift zones are complex assemblages that include *en echelon* zones of eruptive fissures and open fractures underlain by dykes and containing central volcanoes, many of which have multiple calderas and high-temperature geothermal areas. They are blanketed by thick sequences of basaltic lava flows and subaerial and subglacial tuffs and hyaloclastites and are intensely intruded by gabbros. Tertiary areas were built up in the same fashion and thus have the same characteristics, though older.

The nature of the Icelandic crust has been debated for over two decades. During the 1980s, the favoured model involved a hot crust as thin as $\sim$10–15 km, underlain by a layer of partial melt at the top of the mantle. More recently, interpretations of long seismic reflection profiles suggest that the Icelandic crust is thick (25–40 km) and with a distinct Moho at its base. These include the SIST (South Iceland Seismic Tomography) (Bjarnason *et al.* 1993), FIRE (Faeroe–Iceland Ridge Experiment) (Staples *et al.* 1997), B96 (Menke *et al.*

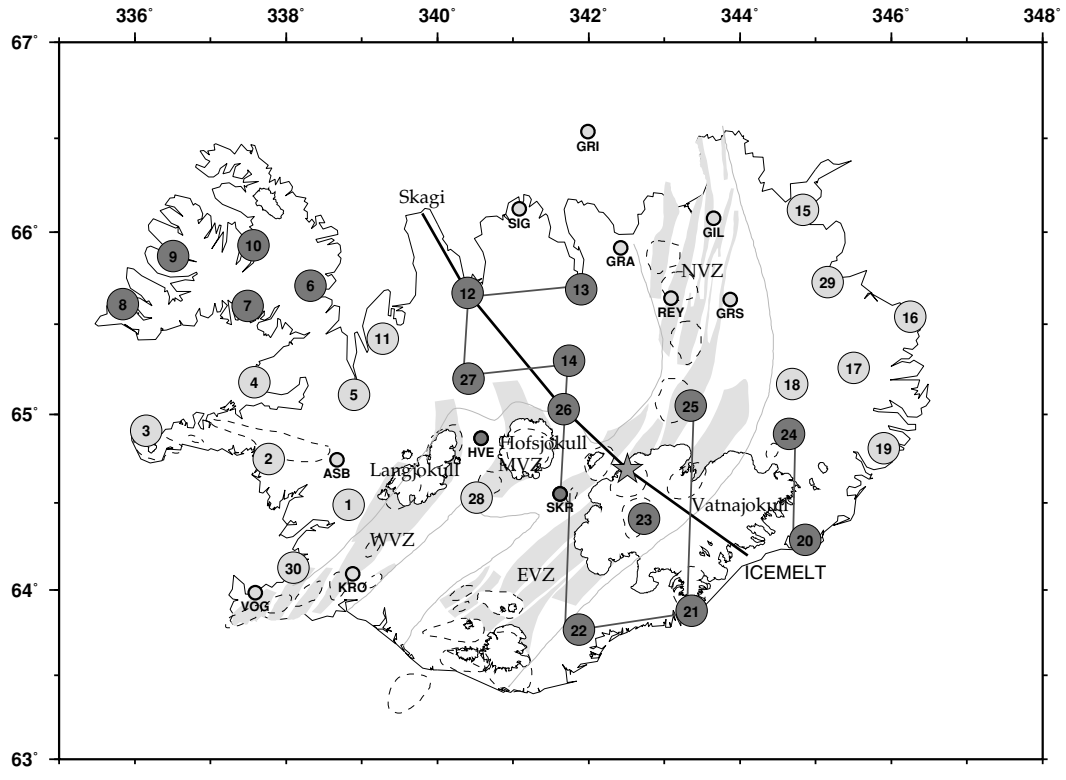

Figure 1. Map of Iceland outlining the neovolcanic zone and showing fissure swarms (grey), central volcanoes (dashed), glaciers (outlined) and the locations of stations of the Iceland Hotspot Project (large dots). Stations of the permanent Icelandic SIL network that had broad-band sensors are shown as small dots. Stations shown in dark grey in central Iceland were used in this study. The five stations studied by Du & Foulger (1999) in the Northwest Fjords are also shown in dark grey. The thick line represents the ICEMELT profile (Darbyshire *et al.* 1998). The grey lines show the station-pair ray paths used to measure Rayleigh wave differential phase velocities. The star shows the location of the Bardarbunga earthquake of 1996 September 29, $M_w = 5.6$. WVZ: Western Volcanic Zone; MVZ: Middle Volcanic Zone; NVZ: Northern Volcanic Zone; EVZ: Eastern Volcanic Zone.

1998) and ICEMELT profiles (Darbyshire *et al.* 1998). In the light of these new results, the RRISP profile, shot in 1977, and on which the thin-crust model was heavily based, was reinterpreted by Menke *et al.* (1996). That reinterpretation suggested that the RRISP profile had originally been incorrectly interpreted by Gebrande *et al.* (1980) and that a Moho at 30–35 km depth below central Iceland was in fact detected by the profile.

The results of these new explosion seismology profiles need to be tested using other kinds of geophysical data. Moho detections made by seismic profiling in Iceland are largely from reflected arrivals, head waves are rare, and despite the relatively large number of long profiles shot, sampling of the deep reflector has only been achieved in a few localities. Explosion profiling suffers the major disadvantage that the rays observed only sample approximately linear zones along a single back-azimuth, and the sampling of deep reflectors is often limited to a small distance range where shot-to-receiver paths are long. In the case of the recent profiles in Iceland, only a few rays turned at great depths, deeper regions were not well sampled, and the majority of the Moho depths were determined using trial-and-error forward ray-tracing modelling along the profile (e.g. Bjarnason *et al.* 1993; Darbyshire *et al.* 1998). Also, because of the geological heterogeneity of Iceland, it cannot be assumed that the structure on either side of a profile is the same as that along the profile trend.

Earthquake seismology provides a powerful complement to explosion seismic profiling. The use of receiver functions to determine crustal structure beneath a three-component broad-band seismograph is now a well-established technique. The method utilizes the waveforms of *Ps* conversions from structural discontinuities beneath the station to model variations in the shear velocity structure of the crust (Ammon *et al.* 1990). Receiver functions sample substantial volumes of the crust around and beneath stations, and earthquakes approaching from several different backazimuths can be used. The method is powerful for detecting velocity discontinuities, in particular the Moho. However, it suffers from the fundamental disadvantage that it can only detect the velocity–depth product, not absolute velocity, and independent constraints on absolute velocity from other *a priori* geophysical sources must thus be used.

Du & Foulger (1999) studied the crustal structure beneath the Northwest Fjords area of Iceland by simultaneously inverting and modelling receiver functions and surface waves. Surface wave phase velocities, measured between station pairs, were used to constrain the average shear wave velocity (V_s) structure of the crust in the neighbourhood of each station. The results showed considerable variation in the nature of the crust and its base in this part of Iceland. Du & Foulger (1999) highlighted two end-member structural types, which they termed structures of the first and second types. Structures of the first type are characterized by a clear tripartite division into an

upper crust with gradients in V_s up to ~ 0.8 s^{-1}, a lower crust with gradients < 0.02 s^{-1}, and a crust–mantle transition zone a few kilometres thick where the velocity gradients increased again to up to ~ 0.2 s^{-1}. Structures of the second type lacked this clear tripartite division; instead, to first order, the velocity gradient decreased smoothly with depth. Many structures obtained fell between these two extreme end-members, showing some characteristics of both.

In general, structures of the first type were best developed in younger, landward areas, whereas structures of the extreme second type were mostly observed beneath older areas. Du & Foulger (1999) took the bases of the upper and lower crust respectively to be the levels where V_s reached 3.7 km s^{-1} (corresponding to a compressional wave velocity V_p of 6.5 km s^{-1}) and where it consistently exceeded 4.1 km s^{-1} (corresponding to a V_p of 7.2 km s^{-1}). These values are the average velocities found for the bases of the upper and lower crusts from explosion profiles throughout Iceland. The base of the lower crust in Iceland does not appear everywhere to be associated with a clear feature such as a sharp, substantial velocity discontinuity or a thin zone with strong velocity gradient. The upper crust was found to tend to thin towards the local extinct rift zone that built the western fjords, whereas the lower crust thickened, in agreement with predictions from kinematic crustal accretion modelling (Palmason 1980). In some cases, anomalously high velocities were detected at shallow depth, and attributed to nearby extinct volcanoes.

Du & Foulger (1999) applied the joint receiver function and surface wave method to an area unexplored by deep refraction profiling. In this paper, we study an area well explored by refraction and wide-angle reflection work. We study a swathe of stations traversing central Iceland and lying along and flanking the recent ICEMELT explosion seismic profile (Fig. 1; Darbyshire *et al.* 1998). This 310 km long, 60-station profile was shot in 1995, and traversed Iceland from the Skagi peninsula across central Iceland and Vatnajokull to the south coast. Six shots were fired, including two powerful end shots, which were recorded along almost the whole length of the profile. The results indicated distinct upper and lower crusts everywhere. The upper crust, the base of which was taken to be the 6.4 km s^{-1} horizon, was found to have a two-layered structure in the north and a thickness of 5–6 km. It thickened to 10 km to the south, beneath central Iceland, but thinned again to less than 3 km beneath Vatnajokull. Southeast of Vatnajokull, on the coast, the structure was similar to that beneath the far north of the profile. The base of the lower crust was interpreted to be characterized by a sharp, reflective Moho with a velocity contrast of 0.5–0.8 km s^{-1}. This reflector was modelled to lie at 25 km depth beneath the north part of the profile, but at 38–40 km beneath Vatnajokull. The velocity at the base of the lower crust was modelled to be 7.1 km s^{-1} beneath the northern end of the profile and 7.2 km s^{-1} beneath the southern part.

We start our inversions using initial starting models determined from the ICEMELT profile. We determine 1-D structural models beneath each station using a combination of receiver function inversion and forward modelling of surface wave dispersion curves. In some cases a significant structural difference may exist between the station locality and its neighbourhood, bringing into question the validity of using interstation surface wave dispersion curves from station pairs to constrain average velocities. In this study, we address this potential problem by, in addition to using surface wave data, constraining our results by directly modelling waveform data up to periods of 1–5 s from a large, local earthquake.

DATA AND METHODOLOGY

Data

The seismograms used in this study were recorded on stations deployed in Iceland in 1996–1998 by the Iceland Hotspot Project. As part of this project, a 35-station network of broad-band seismic stations was operated over the whole of Iceland (e.g. Du & Foulger 1999). The objective of the network deployment was to collect a large set of seismic recordings with which to study the structure of the crust and upper mantle beneath the Iceland hotspot. The seismic stations were all equipped with three-component Guralp CMG-3ESP, 3T or 40T seismometers that have a flat velocity response in the frequency range 0.02 to 30–100 Hz. The data from 30 of the stations were recorded on Refraction Technology 72a-02 24-bit data loggers that recorded at 20 samples s^{-1}. The other five instruments were installed in vaults of the permanent Icelandic SIL network, which recorded at a sampling rate of 100 samples s^{-1}. Absolute timing was provided by GPS at all stations.

We analysed 42 teleseismic events recorded at 12 stations, two of which were deployed in SIL vaults (Fig. 1). The events used cluster in three backazimuths: north (backazimuths of $\alpha = 0°$–$35°$ and epicentral distances of $\Delta = 61°$–$88°$), east ($\alpha = 67°$–$115°$ and $\Delta = 36°$–$73°$) and southwest ($\alpha = 228°$–$271°$ and $\Delta = 62°$–$81°$).

Receiver functions

We use the source-equalization procedure of the frequency-domain receiver function analysis of Langston (1979). A Gaussian low-pass filter with a corner frequency of 1.2 Hz was used to remove high-frequency noise. Most events with magnitudes greater than $M_s = 5.6$ and epicentral distances greater than 35° were useful for our analysis. Deconvolution was carried out using a spectral trough filler, c, of around 0.01–0.001, determined by studying the averaging functions (the vertical component deconvolved from itself, with given c values).

The fact that Iceland is an oceanic island means that microseisms dominate the broad-band seismograms, and stacking of the receiver functions was used to mitigate as much as possible the noise in the data. Since receiver functions corresponding to events from different distances have large amplitude differences, we scale the receiver functions to unit amplitude prior to stacking. The overall data quality is better than that of data from the Northwest Fjords area (Du & Foulger 1999) in terms of signal-to-noise ratio. Examples of data from three stations in different parts of the study area are shown in Fig. 2. There is strong coherence in arrivals for different events from similar backazimuths, particularly in the first 10 s. After stacking, those secondary reverberations that are consistent (for example, the phases arriving at 7–12 s from the east and 5–8 s from the north in the radial receiver functions of station HOT23) may be identified. Comparing the noise amplitudes on the stacked traces with those on the individual traces before the *P* arrival in the radial receiver functions (left panels of Fig. 2) reveals a

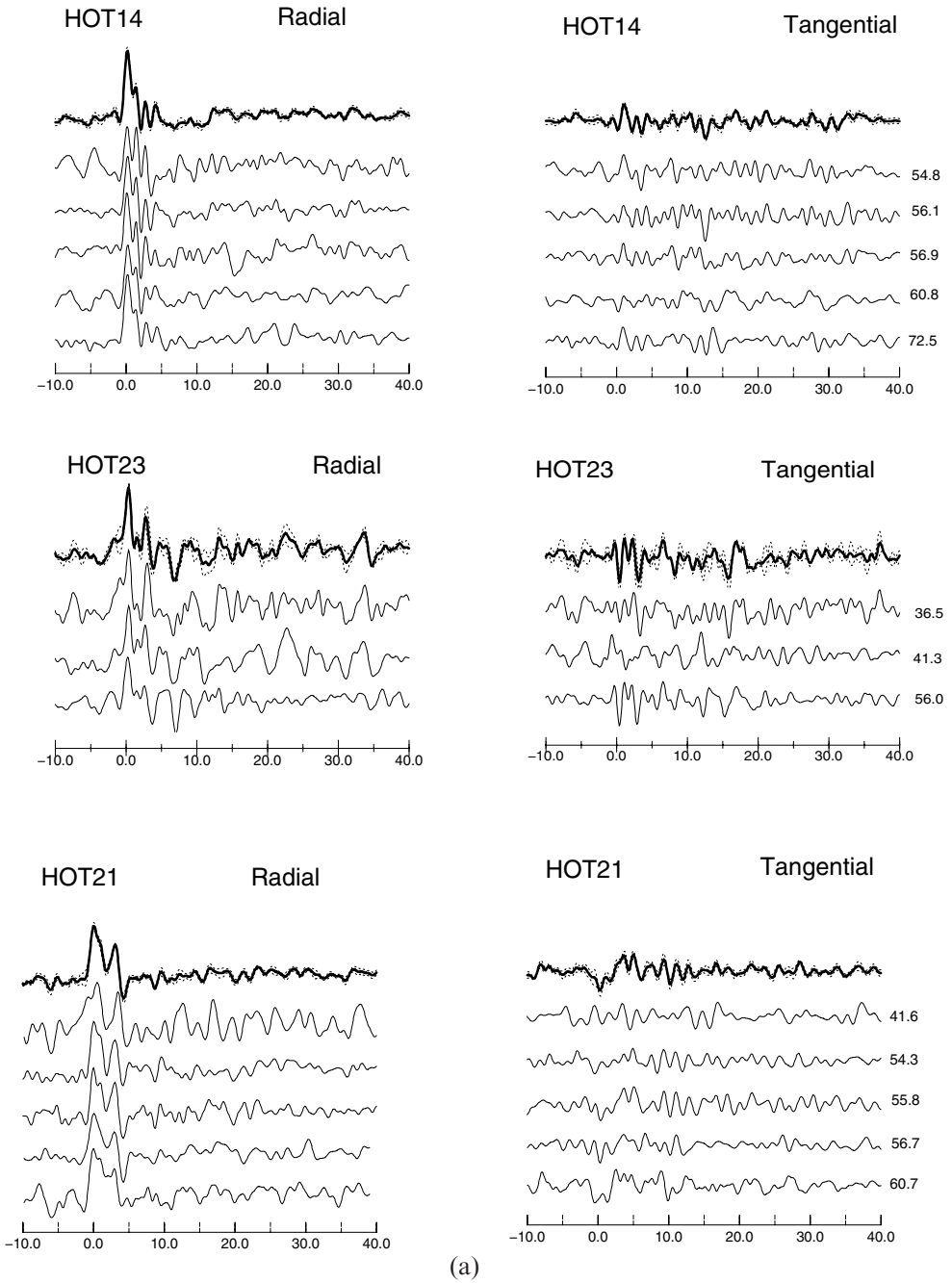

Figure 2. Examples of the stacking of receiver functions for stations HOT14, HOT23 and HOT21. (a) Data from the east backazimuth; (b) data from the north backazimuth. The top trace of each panel shows the stacked receiver function (thick line) and the one standard deviation bounds (dotted lines). Numbers at the right of each trace give the epicentral distances in degrees.

satisfactory level of noise reduction. The stacked tangential receiver functions indicate the level of noise that remains after stacking.

Surface waves

We use three high-quality events with good interstation ray paths (Fig. 1), and measure the surface wave phase velocity dispersion between station pairs. Two events were at teleseismic distances from Iceland and the dominant period band of the surface waves is 25–45 s. Such waves are sensitive to structure deeper than 15 km (e.g. Ozalaybey *et al.* 1997), which is the region of model space that refraction data sample poorly. One event was at a regional distance, has a dominant period of $\sim$15–25 s and samples the shallower structure, which is also sampled well by the wide-angle reflection data. All three events have a high signal-to-noise ratio and high-quality surface wave trains. We analyse the surface wave data using the FTAN (frequency–time domain analysis) package (Levshin *et al.* 1992). The method has the ability to remove interfering, scattered body waves and higher-mode surface waves when extracting the fundamental-mode wave. A detailed description of the method is given by Levshin *et al.* (1992). We use this package to measure interstation pair surface wave phase velocity dispersion curves

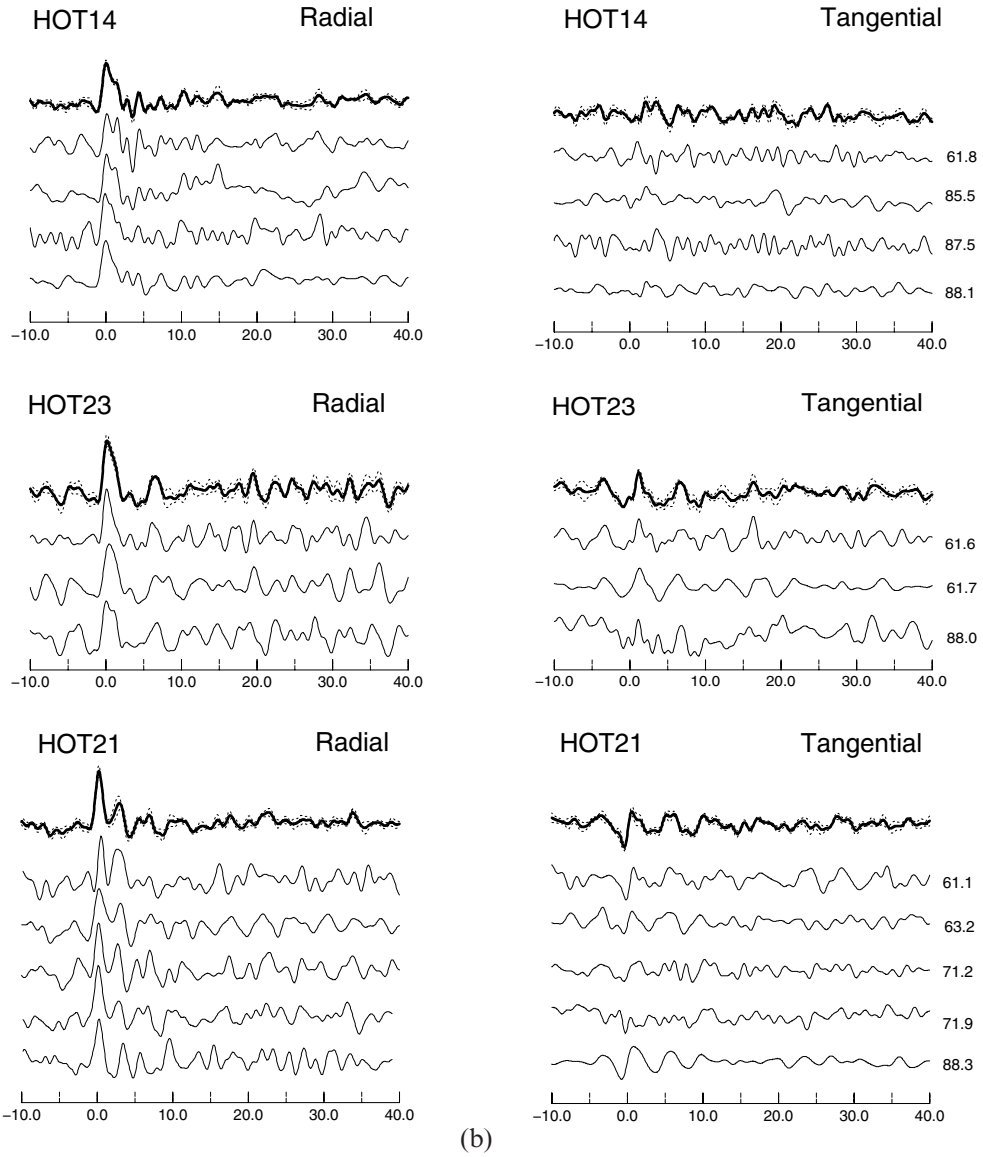

Figure 2. (*Continued.*)

as described by Du & Foulger (1999). The error associated with the measurements is approximately ± 0.1 km s^{-1} (Levshin *et al.* 1992; Du & Foulger 1999), which is close to the scatter in the measured phase velocities between station pairs. For the event from the north backazimuth (E97.339.113217, backazimuth $\alpha = 0.3°$) we measured five fundamental Rayleigh wave interstation differential phase velocity curves (Fig. 3a). Paths HOT21–HOT25 and HOT22-SKR lie mostly within the EVZ and NVZ. The surface wave dispersion curves for HOT22-SKR and HOT21–HOT25 show exceptionally low velocities, which is to be expected in the neovolcanic zone. The path HOT21–HOT25 is also influenced by structural complexities beneath the southern part of the NVZ, which contains a cluster of major central volcanoes. The presence of the Vatnajokull icecap along this path will also tend to lower phase velocities at periods of up to ~ 32 s. The other three north-trending interstation paths yield dispersion curves with much higher velocities that are more characteristic of a continental style of structure. Structural variations are also shown by the three dispersion curves measured using event E97.130.080218 ($\alpha = 85.2°$) from the east backazimuth (Fig. 3b). For periods up to ~ 35 s, path HOT12–HOT13 is characterized by the highest phase velocities, whereas path HOT22–HOT21 yields the lowest phase velocities. Overall, there is a general tendency for the surface wave phase velocities to increase towards the north. Fig. 3(c) shows two dispersion curves at short periods for the north–south-oriented paths of a regional event (E97.178.044058, $\alpha = 186.3°$). These curves reflect the shallow structural complexities that characterize paths HOT12–HOT27 and HOT24–HOT20.

Method

We determine the crustal structure below each station using a combination of receiver function inversion and forward modelling of surface wave phase velocity dispersion curves and the waveforms of a large local event. Combination of these different data provides a robust constraint on the V_s structure of the crust that is superior to either method used in isolation.

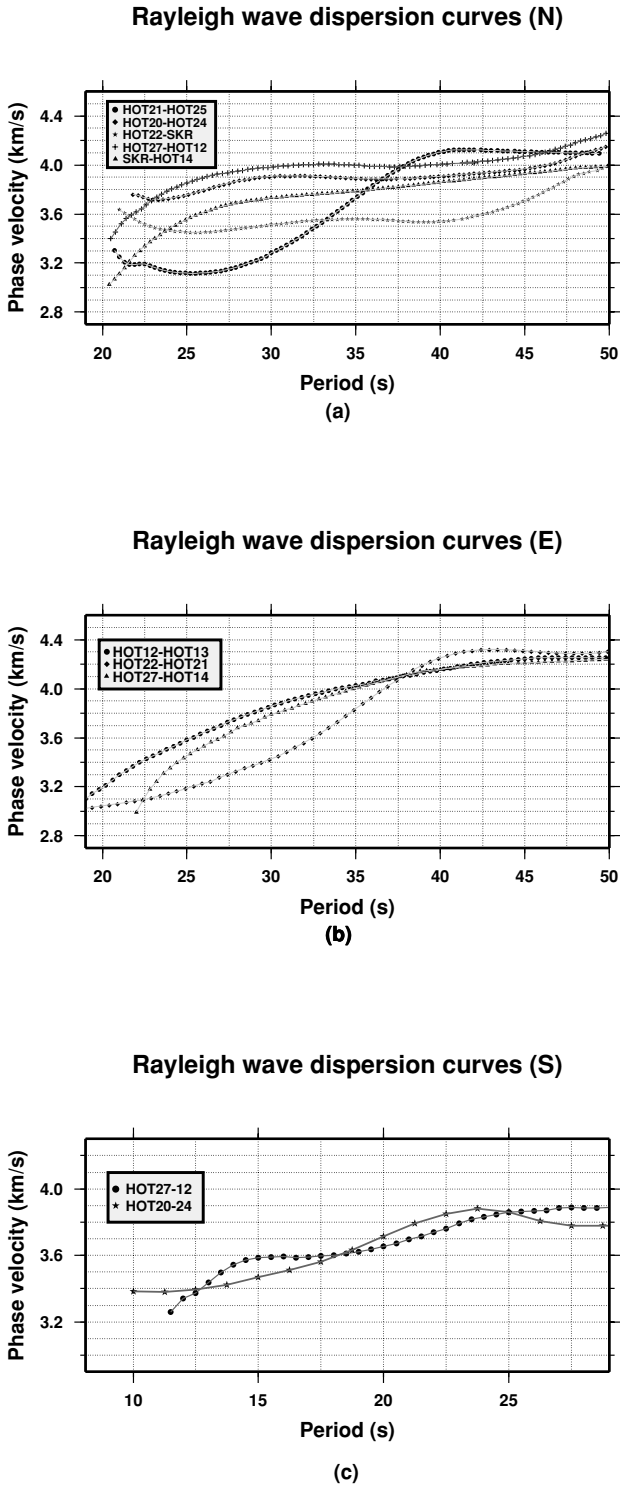

Figure 3. Interstation Rayleigh wave phase velocity dispersion curves. (a) North–south path orientation, measured using event E97.339.113217 ($M_s = 7.7$, $\delta = 58.5°$) from the east coast of Kamchatka; (b) east–west path orientation, measured using event E97.130.080218 ($M_s = 7.3$, $\delta = 53.9°$) from north Iran; (c) north–south path orientation, measured using regional event E97.178.044058 ($M_s = 5.6$, $\delta = 27°$).

We employ the receiver function inversion method of Ammon *et al.* (1990). The method adopts a local linearization of the misfit function, which requires an initial model close to the real crustal structure. We use *a priori* structural information from the ICEMELT profile (Darbyshire *et al.* 1998). We start the inversion using the ICEMELT model as the initial starting model, which we parametrize as a stack of thin layers, 0.5–1.0 km thick for the first 5 km and 2.0–2.5 km thick for deeper layers. We place a half-space below a depth of 50–60 km. The inversion involves two steps (Du & Foulger 1999). We adopt a generic global search method (Du & Foulger 1999) to reduce the dependence of the inversion convergence on the form of the background starting model. We first perturb the starting models with a maximum cubic perturbation of 0.75 km s^{-1} (maximum cubic vector amplitude) and a maximum random perturbation of 0.20 km s^{-1} (V_s distribution variance) using the approach of Ammon *et al.* (1990). We thus invert, at each station, over 75 trial models that vary broadly throughout the entire depth range. We select those models whose synthetic receiver functions lie within or close to the $\pm 1\sigma$ bounds of the most significant observed phases, use them to compute theoretical surface wave dispersion curves, and compare the results with the observed curves. The few models that match the dispersion curves to within less than ± 0.2 km s^{-1} are selected and used in the second step. In this step, we conduct a suite of receiver function inversions with a varying smooth weighting, using the same number of iterations and solution roughness parameters as used in the first step. We finally take the smoothest model that can fit the surface wave dispersion curves to within or close to ± 0.1 km s^{-1}. Where we suspect structural heterogeneity in the vicinity of the station, bringing into question the validity of using interstation surface wave dispersion curves to constrain the average velocities, we use for the second step models obtained using forward waveform modelling and direct comparison with seismograms observed at the stations. This procedure is described in detail in the following section.

We present our results as a set of velocity–depth profiles for V_p. Receiver function analysis yields V_s, and we construct our profiles by converting this to V_p using a V_p/V_s ratio of 1.76 (Menke *et al.* 1996), which is a typical value for the Icelandic crust as a whole (Darbyshire *et al.* 1998).

RESULTS

Crustal structure beneath stations HOT12 and HOT13

Stations HOT12 and HOT13 lie to the north within the Tertiary Trollaskagi block, and station HOT12 lies very close to the ICEMELT profile. Stacked receiver functions were constructed for three backazimuths. The second step of each receiver function inversion is based on models that already lie in the model space defined by the ± 0.2 km boundaries of the surface wave dispersion curves. The second-step receiver function inversions further improve the model fits by adding fine structural detail. The lower right-hand panels of Figs 4 and 5 summarize the inversion results, giving the three smoothest models from each backazimuthal inversion and an overall average model. Fig. 6 compares the surface wave dispersion curves measured for paths HOT27–HOT12 and HOT12–HOT13 to the predicted dispersion curves of the average models determined for stations HOT12 and HOT13. There is significant improvement and the predicted curves fit the observed curves to within or close to the ~ 0.1 km error bounds. Although the average models fit the long-period surface wave data well, near-station structures may significantly influence short-period Rayleigh waves. Fig. 6(a) shows that the agreement between a

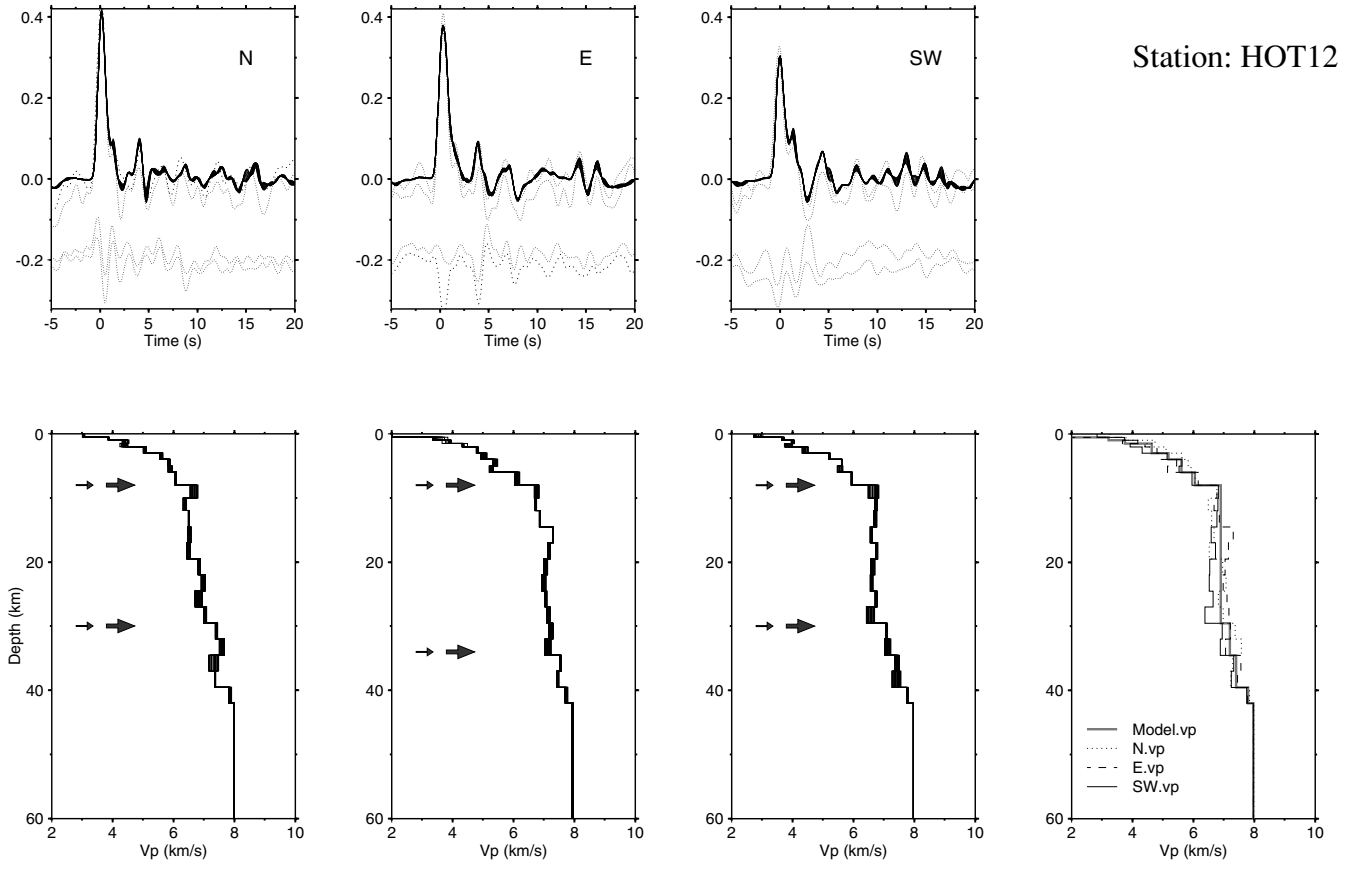

Figure 4. Receiver function inversion results for station HOT12. Upper panels show measured $\pm 1\sigma$ bounds of the radial (top) and tangential (bottom) receiver function data (dotted lines) and synthetic radial receiver functions computed from each inversion solution model (bundle of solid lines). Lower panels show the inversion solution models. The lower right-hand panel shows a summary of the inversion in the form of the smoothest model from each backazimuth (thin solid, dotted and dashed lines) and an overall average model (thick grey line). Small arrows show the depths at which V_p reaches 6.5 km s^{-1} and the depth below which it does not fall below 7.2 km s^{-1}. Large arrows show the best estimates of the depths to the bases of the upper and lower crusts. The V_s models derived from the receiver function analysis are converted to V_p using a V_p/V_s ratio of 1.76 (Menke *et al.* 1996).

short-period ($\sim$11–27 s) dispersion curve for path HOT27–HOT12 and the predictions of the smoothest north-azimuth models for stations HOT12 and HOT27 is satisfactory.

We assume that the base of the upper crust is the shallowest level at which V_p reaches $\sim$6.5 km s^{-1}, and that the base of the lower crust is the level below which V_p does not fall below $\sim$7.2 km s^{-1}. The inversion results for stations HOT12 and HOT13 are broadly similar, suggesting that they lie in a relatively homogeneous region. The upper crust has a thickness of $\sim$8 km beneath both stations. It is characterized by velocity gradients of up to $\sim$0.7 s^{-1} in the upper few kilometres and much less at deeper levels. Comparing this with the result of the ICEMELT profile suggests that the upper crust we identify probably corresponds to the bipartite upper crust determined by forward modelling of the ICEMELT data (Darbyshire *et al.* 1998), which yielded a depth to the base of the upper crust of $\sim$5 km. However, that modelling assumed a velocity horizon of 6.4 km s^{-1} for the base of the upper crust, slightly lower than the 6.5 km s^{-1} we assume. The lower crust has much lower velocity gradients, and the results from different backazimuths place its base at 30–34 km beneath station HOT12. This is very close to the depth of $\sim$28 km obtained from the ICEMELT profile, given that there are depth uncertainties of $\pm$2 km in the ICEMELT determinations (Darbyshire *et al.* 1998) and $\pm$2.5 km in our receiver function results (the layer thickness near to the base of the lower crust), and that the velocity at the base of the crust was taken to be 7.1 km s^{-1} in modelling the ICEMELT data. The depths obtained using the data along the trend of the ICEMELT profile and from the south-west backazimuth are 30 km, in excellent agreement with the ICEMELT result. Some model discrepancies are, nonetheless, not unexpected, since the ICEMELT experiment yielded a V_p structure directly, whereas receiver functions yield a V_s model that must be converted to V_p by assuming a value for Poisson's ratio. Beneath station HOT13 the base of the lower crust lies at a depth of 28–30 km. The clarity of the upper and lower crustal subdivisions varies beneath the two stations, with structures of the second type obtained from inversion of data from the north backazimuth and structures of the first type from data from the southwest backazimuth.

The radial receiver functions of station HOT12 show a coherent, large-amplitude positive arrival at $\sim$3.5 s (upper panels of Fig. 4). This is the *Ps* arrival from the thick zone with high velocity gradient at $\sim$30–34 km depth at the base of the lower crust (lower panels of Fig. 4). This zone is best developed in the structure obtained from the data from the southwest

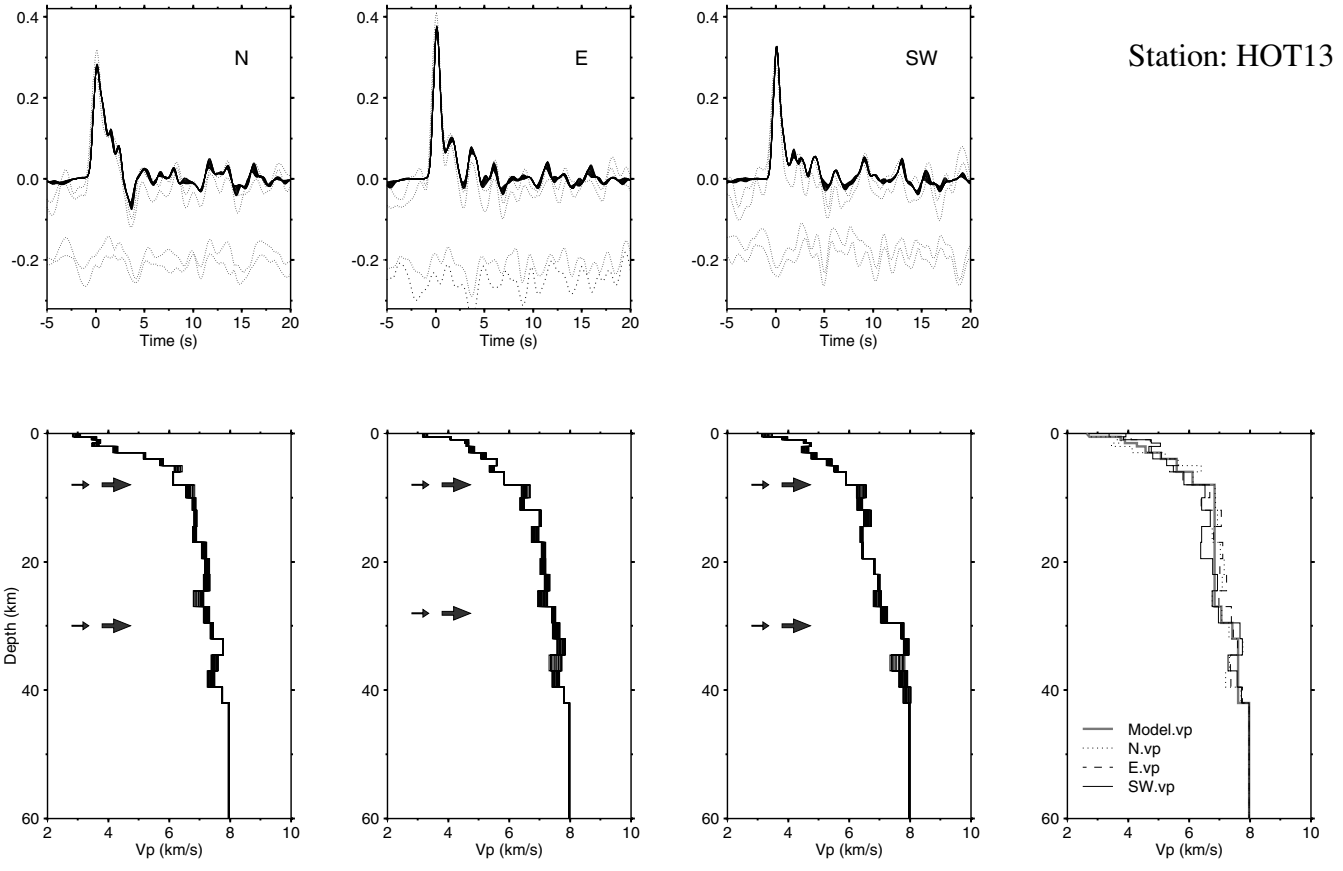

Figure 5. Same as Fig. 4 but for station HOT13.

backazimuth. The radial receiver functions of station HOT13 show a coherent positive arrival at ~1.5 s, which is probably the *Ps* conversion from the base of the upper crust at a depth of ~8 km. There is also a *Ps* phase at ~3.5 s, which is clear in the radial receiver functions for the east and south-west backazimuths but which merges with a negative arrival for the north backazimuth. This apparent negative arrival is probably the multiple PpS_hs generated from the base of the upper crust. It has a lower amplitude in the data from the other two backazimuths. The radial receiver functions have large amplitudes compared with the pre-signal noise and their tangential counterparts, and the fits to the models obtained are satisfactory.

Crustal structure beneath stations HOT27 and HOT14

Stations HOT27 and HOT14 lie southerly in the Trollaskagi block. Station HOT14 has data from only two backazimuths (upper panels of Fig. 7). The radial receiver functions have a double peak at ~2.7–4.0 s, and the *Ps* arrival from the base

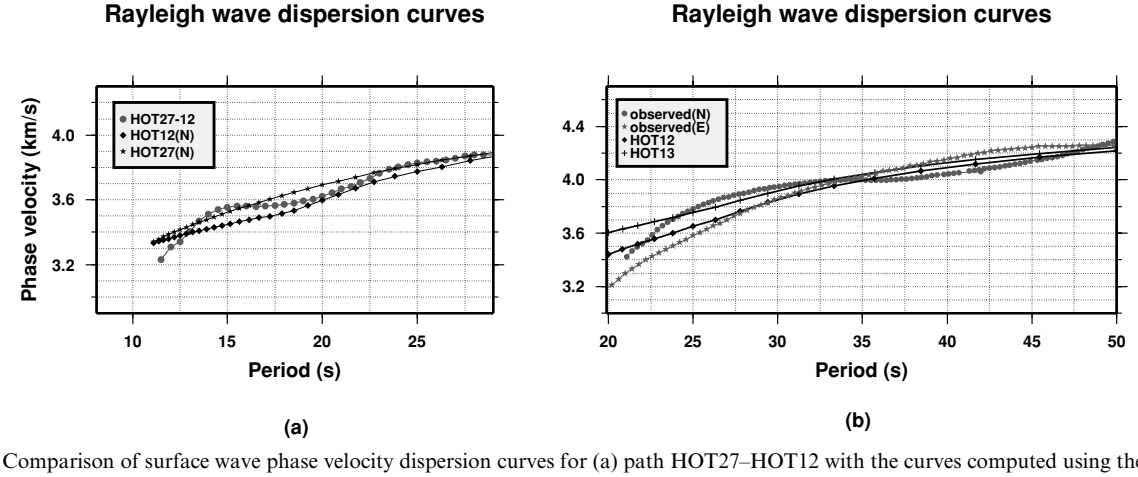

Figure 6. Comparison of surface wave phase velocity dispersion curves for (a) path HOT27–HOT12 with the curves computed using the smoothest north backazimuthal models of stations HOT12 and HOT27, and (b) the north–south path HOT27–HOT12 and the east–west path HOT12–HOT13 and the predictions of the two average models for stations HOT12 and HOT13.

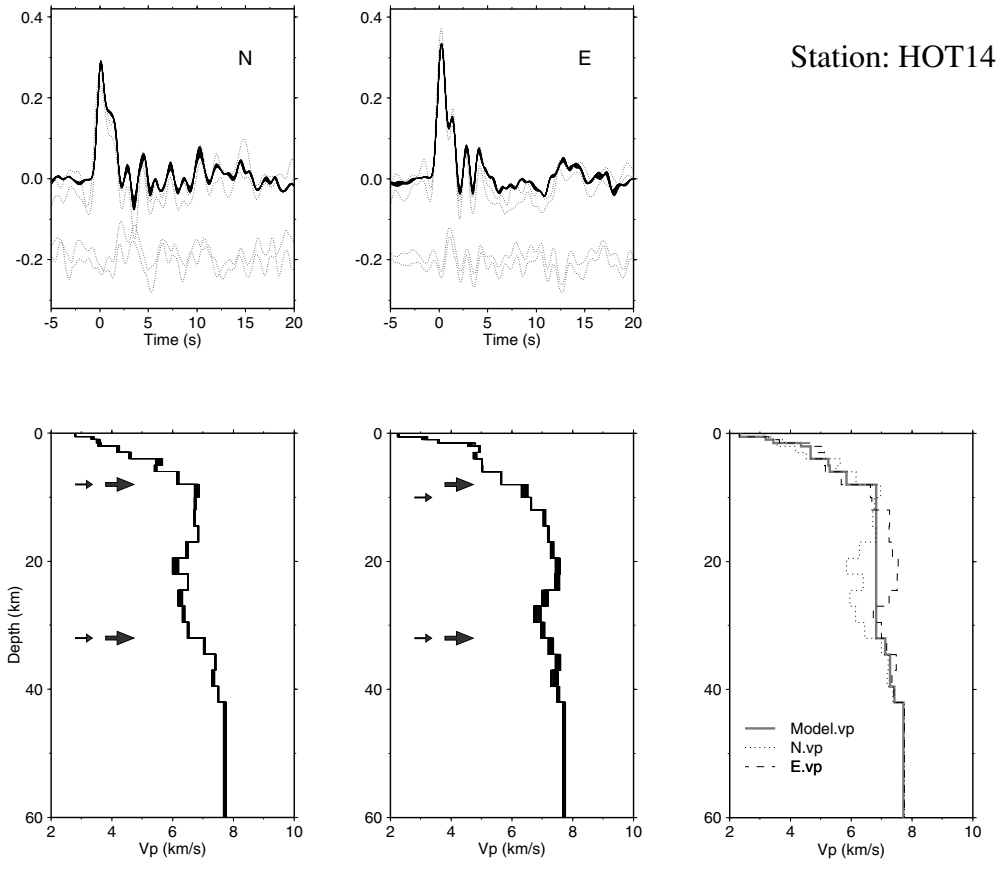

Figure 7. Same as Fig. 4 but for station HOT14.

of the lower crust interferes with the converted phases and reverberations from a low-velocity zone (LVZ) just above. Data from all three backazimuths are available for station HOT27 (Fig. 8). The radial receiver functions for this station show clear *Ps* conversions at about 3.5 s followed by a broad positive arrival at ~10–13 s. This is PpP_ms, the multiple generated from the base of the lower crust.

The resultant structures are broadly similar for these two stations. The majority show type 1 structures, with clear demarcation of the upper crust, the lower crust and the crust–mantle transition. The base of the upper crust is at ~8 km beneath station HOT14 and at 8–10 km beneath station HOT27. A best estimate for the depth to the base of the lower crust is ~32 km beneath station HOT14 and ~28–30 km beneath station HOT27. There is a systematic backazimuthal structural variation in that the data from the east backazimuth yield higher velocities for the lower crust than the data from the north backazimuth. This is well developed under station HOT14, and may explain the phase reversal at ~2–6 s in the tangential receiver functions for this station. The inversion results for both backazimuths show good agreement with the observed surface wave phase velocity dispersion curves (Fig. 9).

Crustal structure beneath stations HOT26, HVE and SKR

Stations HOT26, HVE and SKR are located in the MVZ in the centre of Iceland. Only data from the east backazimuth are available for station HOT26, but data from the southwest backazimuth are also available for stations HVE and SKR (upper panels of Figs 10a and 10b). The radial receiver function for station HOT26 has a prominent trough at ~6 s. This is also present in the east backazimuth radial receiver function for station HVE, but with a lower amplitude. The radial receiver functions for the east backazimuth data for stations SKR and HVE have a high-amplitude trough at ~2 s and high-amplitude peaks *Ps* at ~3–4 s, respectively. Their southwest backazimuth radial receiver functions feature a pair of peaks at ~3 and ~6 s.

The structural models obtained by inversion show some general similarities. In particular an LVZ is consistently obtained for the lower crust (lower panels of Figs 10a and b). Depths to the base of the upper crust all lie in the range ~5–10 km, and beneath this velocities increase somewhat. At greater depth, however, velocities decrease again, in extreme cases to fall below 6 km s^{-1}. The depth to the base of the lower crust is consistently determined to be at 35–40 km depth. The ICEMELT profile passes very close to station HOT26. Here, a depth to the base of the upper crust of ~8 km is determined, compared with a value of 10 km for the ICEMELT profile. Moho reflections were not seen at this point along the ICEMELT profile, but extrapolation from adjacent areas suggests a depth of ~40 km. The agreement with our results is thus satisfactory, although the LVZ we observe is not modelled by Darbyshire *et al.* (1998).

We nevertheless explore the requirement of our data for the LVZ. In the southwest backazimuth results for stations SKR and HVE, the converted phases and reverberations generated by the LVZ at ~25–30 km depth contribute to the receiver

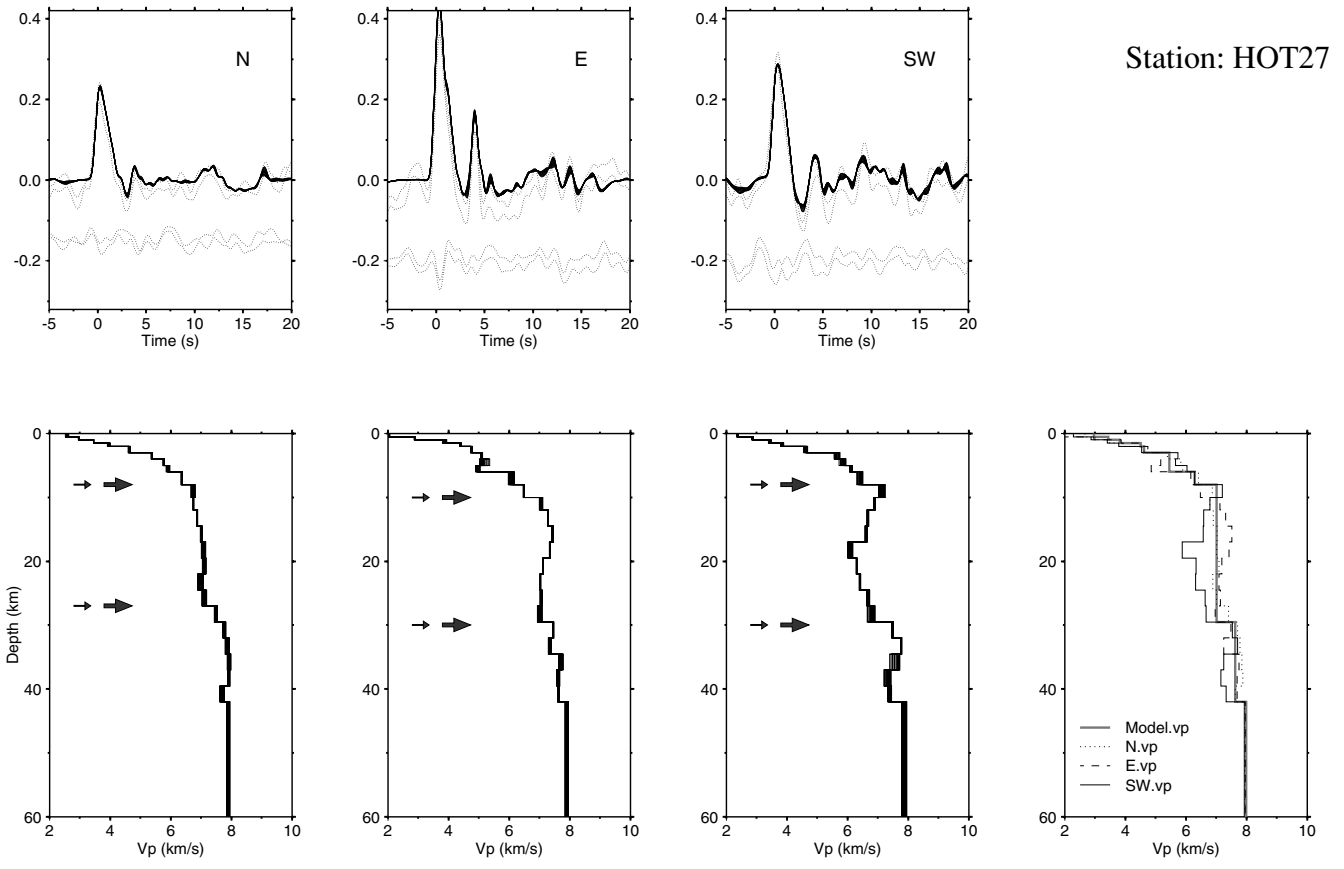

Figure 8. Same as Fig. 4 but for station HOT27.

function wave train after the *Ps* arrival from the crust–mantle transition zone, that is, the large-amplitude positive arrival at 6 s, and the negative arrivals flanking it. The high-amplitude troughs at 2 s in the receiver functions from the east backazimuth are probably the *Ps* conversions from the top of the lower crustal LVZ, and the strong troughs at 6 s in the east backazimuth receiver function of stations HOT26 and HVE are most probably reverberations from structural complexities at depths of ~30–40 km.

An LVZ and structural complexities in the lower crust may not be required if only the early parts of the receiver functions, up to the *Ps* arrival at 3–4 s, are modelled. Fig. 10(c) shows simplified results, where later parts of the receiver function are not modelled, a procedure used by Mangino *et al.*, (1999). Darbyshire *et al.* (2000) adopted a similar approach in modelling noisy receiver functions from single earthquakes recorded in Iceland. They found two minor LVZs beneath station HVE between 7 and 18 km depth from inverting a

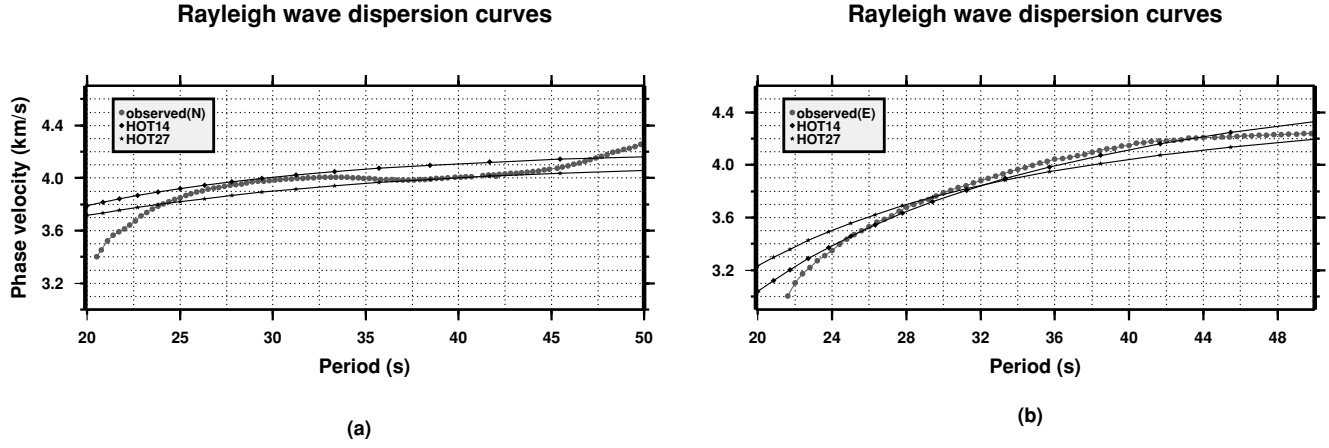

Figure 9. Comparison of surface wave phase velocity dispersion curves with the predicted curves for the average models of stations HOT14 and HOT27 for (a) the north–south path HOT27–HOT12 and (b) the east–west path HOT27–HOT14.

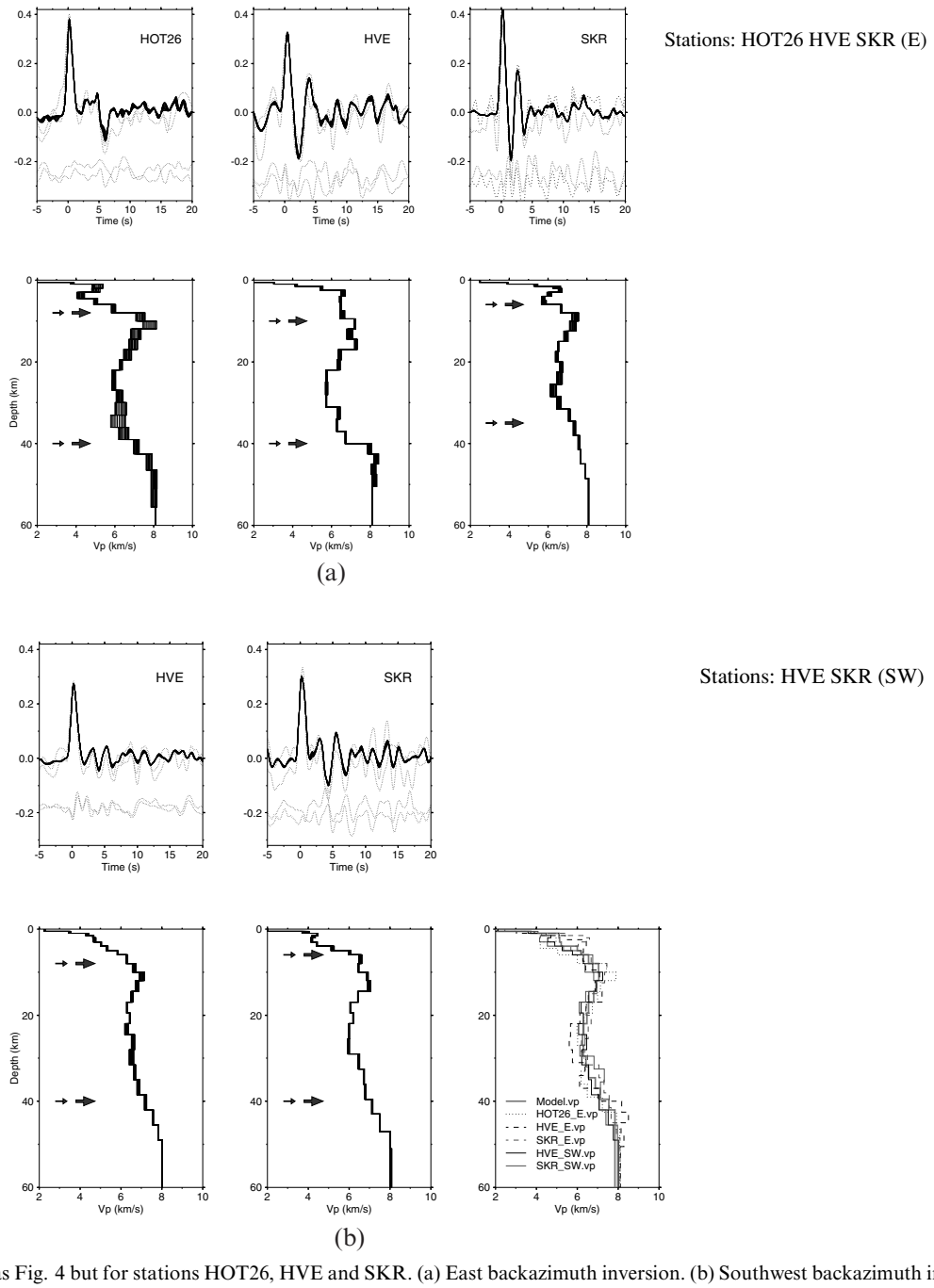

Figure 10. Same as Fig. 4 but for stations HOT26, HVE and SKR. (a) East backazimuth inversion. (b) Southwest backazimuth inversion. The lower right-hand panel of (b) shows the five smoothest models (thin solid, dotted and dashed lines) and an overall average model (thick grey line). (c) Lower panels show simplified versions of the models of (a) without an LVZ. The solid lines in the upper panels denote the synthetic radial receiver functions computed from these simplified models.

southwest backazimuthal receiver function and two minor LVZs between 15 and 30 km depth from inverting an east backazimuthal receiver function. These LVZs could not be constrained well, as the authors pointed out, because the data were limited and contained noise from scattering. Their inversions only provided information as to the likely structural variations beneath station HVE. The major LVZ we identify may be responsible for the poor SKR receiver function fit shown by Darbyshire *et al.* (2000), where even the first *Ps* arrival could not be fitted well. Beneath station SKR, the only reliable features identified by them were a high-velocity 'lid' at 5–8 km depth and a large positive velocity step at $\sim$19 km depth. We also observe these features in our southwest backazimuth result (Fig. 10b). Comparison of Figs 10(a) and (c) shows clearly that models with higher velocity at depths of $\sim$8–15 km and lower velocity at depths of $\sim$20–35 km depth significantly improve the fit to the arrivals in the time interval $\sim$5–15 s. The simplified models leave substantial unmatched energy in the receiver function waveforms. Since it is required by the data, and is shown consistently by five groups of independent receiver function inversions at three different stations, we believe that the crustal low-velocity zone is a robust feature.

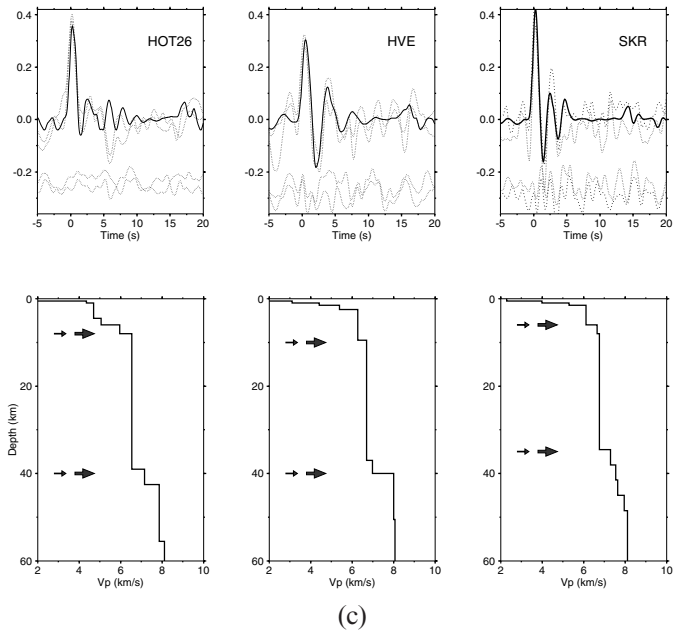

Figure 10. (*Continued.*)

Although the results show very consistently that an LVZ exists in this region, its lateral extent is not constrained. In order to explore this feature further, we model the waveforms of a large, local earthquake. The Bardarbunga earthquake of 1996 September 29, $M_w = 5.6$, occurred in northwest Vatnajokull, and seismic waves traversed the MVZ *en route* to station HOT27. The wave path to station HOT14 lies just outside the area. We compute synthetic seismograms up to 1 Hz using a multi-mode surface wave summation technique (Panza 1985) and using the source mechanism determined by Nettles & Ekstrom (1998). Fig. 11 shows a comparison of the synthetic and observed seismograms. The 1-D structure used for the path to station HOT27 is the average of the five structures determined for stations HOT26, HVE and SKR (Fig. 10b), and the structure used for the path to station HOT14 is the average of the two structures determined for that station (Fig. 7). The wave path to station HOT27 lies partly within the LVZ, but also crosses transversely the EVZ and the MVZ. In such a complex structural

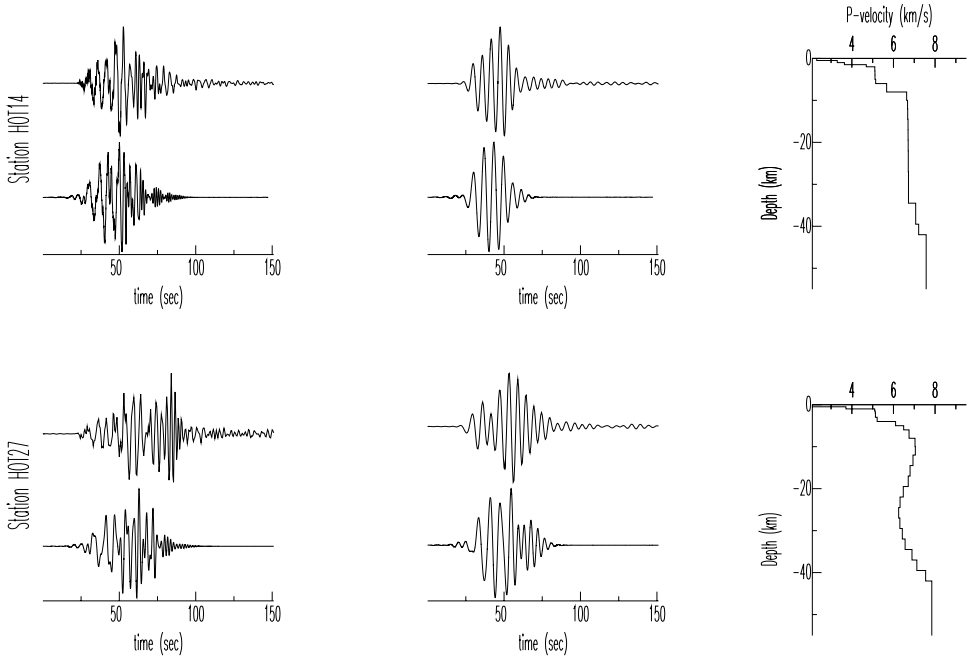

Figure 11. Comparison between observed and synthetic seismograms for the Bardarbunga, Iceland earthquake of 1996 September 29, $M_w = 5.6$. The observed (upper) and synthetic (lower) signals have been low-pass filtered at 1 s (left) and 5 s (middle). The 1-D path-average structures used for computing the synthetic seismograms are shown on the right.

area, as expected the waveform observed at station HOT27 displays a high-amplitude surface wave train influenced by scattering and multipathing at structural discontinuities along its path. Waveform modelling using a 1-D average of the 3-D structure around station HOT27 produces a relatively poor fit to the later parts of the surface wave train (Fig. 11). However, the early parts of the waveforms are reproduced well. The overall quality of the fit is good, even at frequencies as high as 1 s, and the fit improves as the seismograms are progressively low-pass filtered to 5 s. This further confirms that the LVZ beneath the MVZ is a robust feature required by the data. The waveform modelling results for station HOT14 suggest that the LVZ does not extend that far to the east.

Crustal structure beneath stations HOT23 and HOT25

Stations HOT23 and HOT25 are located well within the currently active neovolcanic zone. Station HOT23 was deployed on a nunatak in Vatnajokull that is the caldera rim of the Grimsvotn volcano, one of a cluster of volcanoes in this region, which is the highest and most volcanically productive in Iceland. It lies very close to the ICEMELT profile. Data are available from the north and east backazimuths for both stations (upper panels of Figs 12 and 13a). At $\sim$3 s the east backazimuth radial receiver functions have a large-amplitude peak, which is present at lower amplitude in the north backazimuth radial receiver functions. The north backazimuth radial receiver function of station HOT23 also has a large-amplitude peak at $\sim$6 s, which is present in the north backazimuth radial receiver function of station HOT25 but at a lower amplitude. The waveforms of the east backazimuth tangential receiver functions contain more high-frequency power than their northern counterparts. Since both stations are sited in large central volcanoes, major heterogeneities at the stations may be responsible for these waveform pattern complexities. The models resulting from the inversion exhibit significant backazimuthal variation (lower panels of Figs 12 and 13a), which may also be partly caused by rift anisotropy. Both backazimuthal structures at station HOT25 are of the first type, with an upper crust 5–8 km thick. The depth at which V_p reaches 7.2 km s^{-1} is highly variable, however, being $\sim$25 km for the north backazimuthal data and $\sim$35 km for the east backazimuthal data. For station HOT23, the depth at which V_p reaches 6.5 km s^{-1} is 5 km for the north backazimuthal data and 8 km for the east backazimuthal data. Depths to the 7.2 km s^{-1} horizon are fairly consistent, on the other hand, at 38 and 42 km.

To investigate further the apparently highly variable and anomalous structure in the neighbourhood of station HOT23, the lower crust in the inversion models was simplified and the first-order model features tested using forward modelling (Fig. 13b). Comparison of the synthetic receiver functions with the observed data (upper panels of Fig. 13b) shows that the fit to the north backazimuth data is marginal for most of the wave train, and the fit to the east backazimuth data is very poor after the first 5 s.

Lateral structural variations are also responsible for the variation in the two different backazimuthal radial receiver functions for station HOT25. An adequate fit to the east radial receiver function is not achieved. Because the large volumes sampled by receiver functions are clearly 3-D, we identify

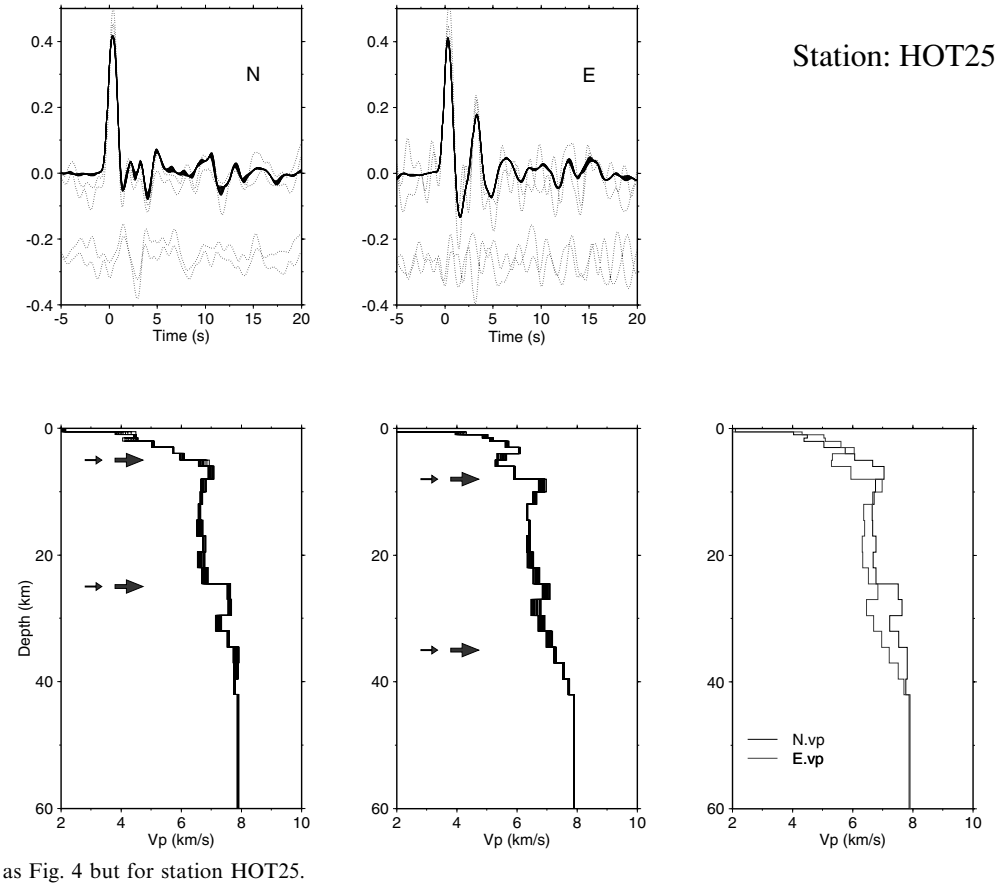

Figure 12. Same as Fig. 4 but for station HOT25.

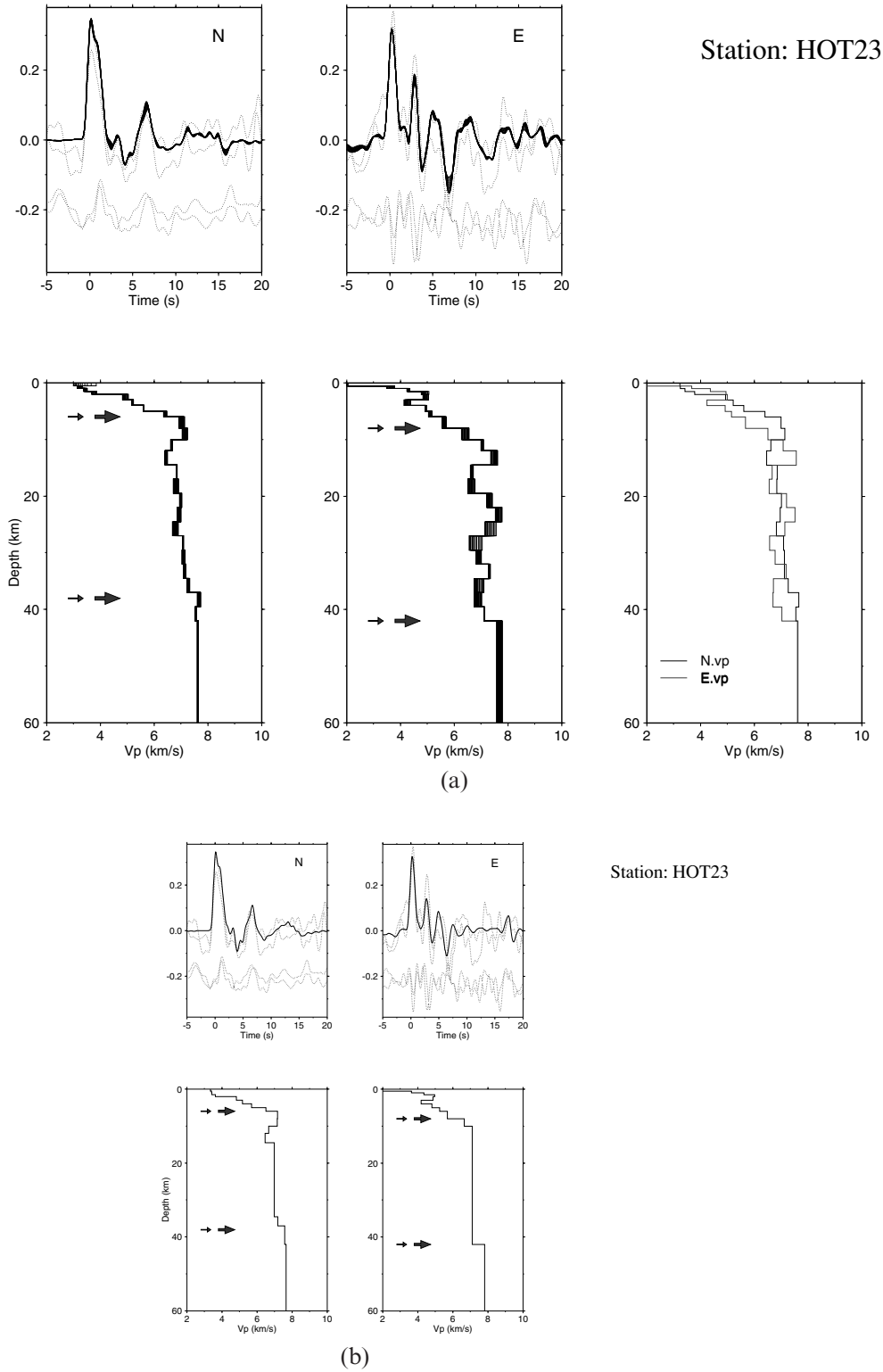

Figure 13. (a) Same as Fig. 4 but for station HOT23. (b) Lower panels show models obtained from simplifying the lower-crustal structures of (a). The solid lines in upper panels denote the synthetic radial receiver functions computed from these simplified models.

which model features are robust for both stations by modelling the waveforms of the Bardarbunga earthquake, which occurred north of station HOT23 and southwest of station HOT25. Fig. 14 shows a comparison of synthetic and observed seismograms at stations HOT23 and HOT25. The 1-D structural models used were from the north backazimuthal data for station HOT23 and from the east backazimuthal data for station HOT25. The fit is good down to periods of 5 s, and in some cases down to 1 s. These two models are thus our preferred results for these stations.

Modelling of the ICEMELT data suggests that the upper crust thins from $\sim$10 km beneath the MVZ to a minimum

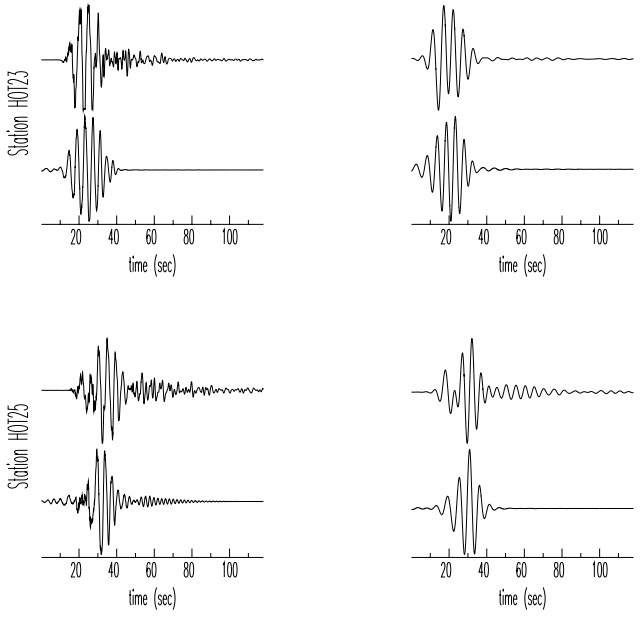

Figure 14. Same as Fig. 11 but for stations HOT23 and HOT25. The 1-D path-average structures used for computing the synthetic seismograms are the smoothest models from the north backazimuth receiver function inversions for station HOT23 and the east backazimuth receiver function inversions for station HOT25 (shown in the lower right-hand panels of Figs 13a and 12 respectively).

of ~3 km beneath northern Vatnajokull. This compares with our result of 5–8 km for the 6.5 km s^{-1} horizon. Darbyshire *et al.* (1998) suggested that their extremely low value is caused by sampling the crust beneath central volcanoes, which are known to be commonly underlain by high-velocity intrusives (e.g. Foulger & Toomey 1989). Our receiver function results for the upper crust agree with those from the ICEMELT profile in so much as we observe a thinning of the upper crust beneath the EVZ (stations SKR, HOT23 and HOT25) compared with the Trollaskagi block. The thicker upper crust we determine for station HOT23 is probably a result of the larger volume averaging inherent in our method. The agreement in the estimates of the depth to the 7.2 km s^{-1} horizon from the receiver function data and the ICEMELT profile is satisfactory.

Crustal structure beneath stations HOT21, HOT20 and HOT24

Stations HOT21 and HOT24 are located on the peripheries of large central volcanoes belonging to the Snaefell Flank Zone. Station HOT20 lies just east of this zone, on Tertiary rocks. The ICEMELT profile passes between stations HOT21 and HOT20 and so direct comparison of results is not possible. Receiver functions are available for all three stations for earthquakes from the north and east backazimuths (Fig. 15). Common features of the radial receiver functions for the north

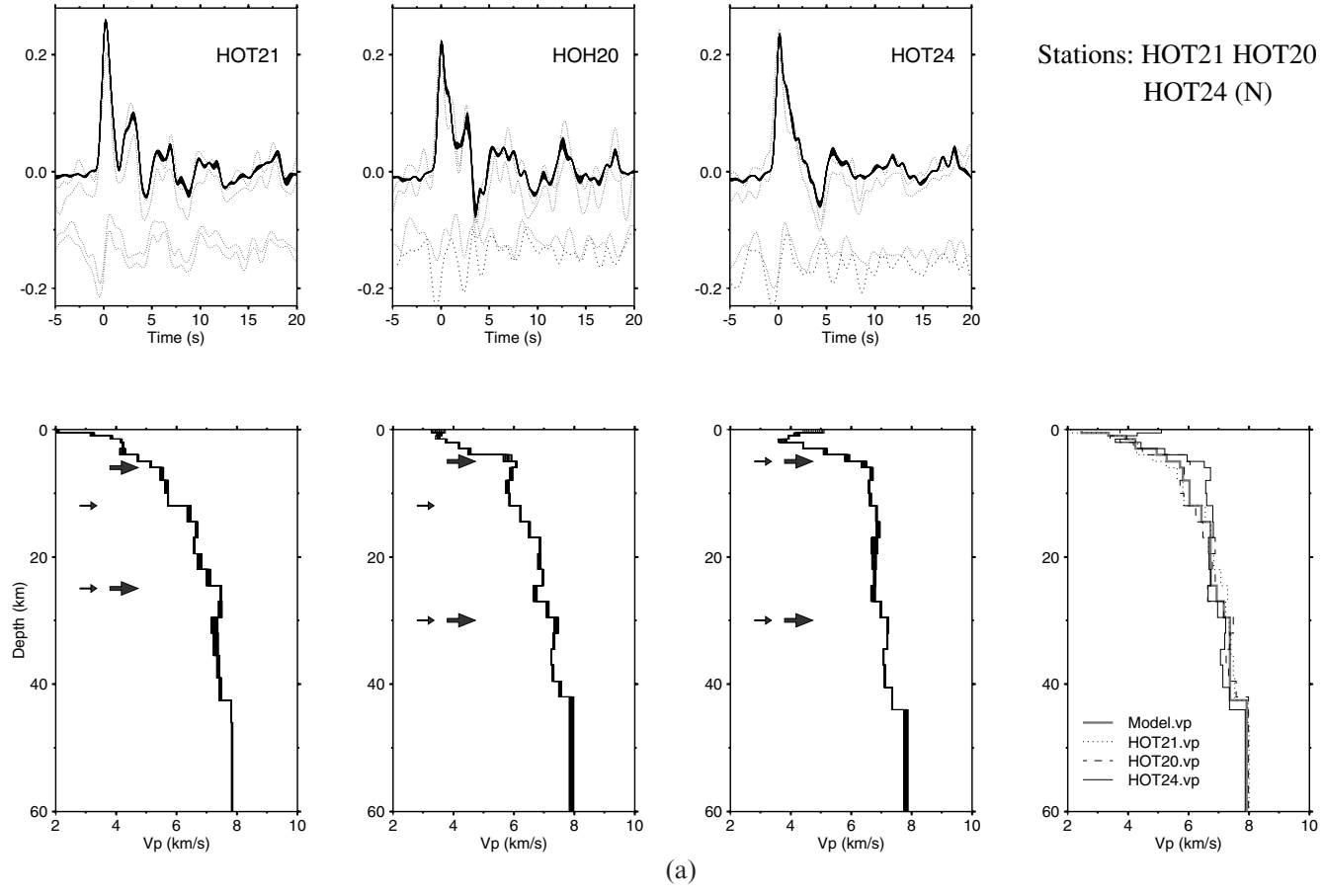

(a)

Figure 15. Same as Fig. 4 but for stations HOT21, HOT20 and HOT24. (a) North backazimuth receiver function inversions; (b) east backazimuth receiver function inversions.

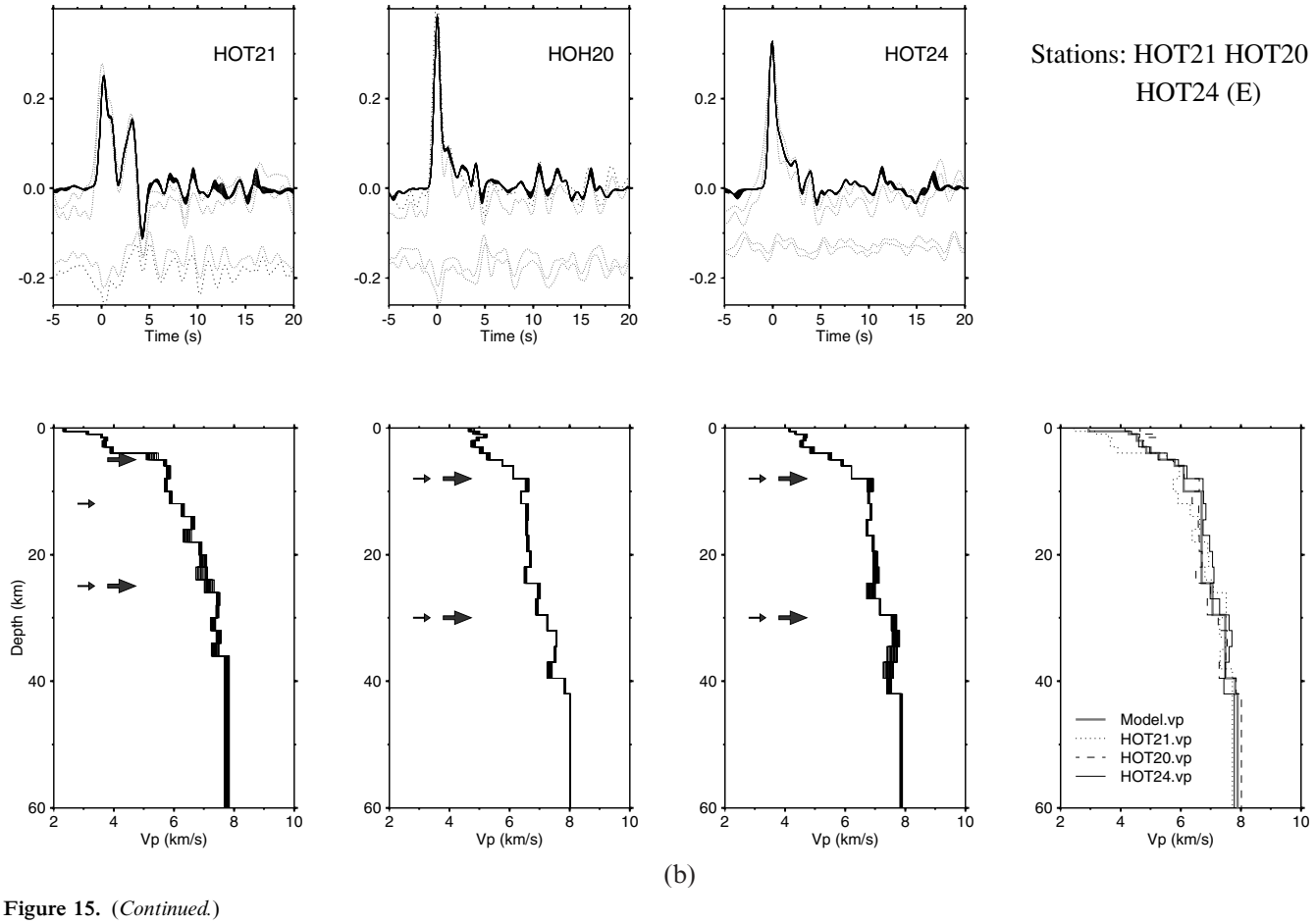

Figure 15. (*Continued.*)

backazimuth data are a double peak starting at ~6 s, a large-amplitude trough at ~4 s and a large-amplitude peak at ~2.5 s, which interferes with the direct *P* arrival (at time zero) in the radial receiver function of station HOT24 (upper panel of Fig. 15a).

The prominent arrival at 2.5 s in the north backazimuth radial receiver functions is probably the *Ps* conversion from a step in the models at ~12 km depth, reinforced by the simultaneous arrival of PpP_hs phases generated at a top discontinuity at ~5 km depth. The negative PpS_hs phase arrival at ~4 s interferes destructively with the *Ps* phase from the base of the lower crust. The pair of peaks at 6–7 s arises from the PpP_is phase ('*i*' represents an intermediate crustal interface) probably generated at the interface at ~12 km depth. The east backazimuth radial receiver functions are variable, but there is a coherent trough at ~4.5 s probably arising from the PpS_hs arrival from the top of the lower crust.

There is some ambiguity in the depth to the base of the upper crust, but consistent features are found in the depth range 5–8 km. The depth at which V_p reaches 7.2 km s^{-1} is at ~25 km beneath station HOT21 and ~30 km beneath stations HOT20 and HOT24.

Figs 16(a) and (b) show comparisons of observed surface wave phase velocity dispersion curves for paths HOT20–HOT24 and HOT22–HOT21 and predicted curves calculated using the average models for each backazimuth for all three stations (lower right-hand panels of Figs 15a and b). The curve predicted using the structures derived from the north backazimuth data fits the observations well. The fit is good even down to periods as short as ~11 s at stations HOT20 and HOT24 (Fig. 16c), but the fit using the structures derived from the east backazimuth data is poor. The surface wave dispersion curve from the interstation path HOT21–HOT22 samples an area west of station HOT21, however, unsampled by receiver functions and distant from stations HOT20 and HOT24. The misfit therefore suggests that there is a significant structural change west of station HOT21. This is likely, since this region contains the most extreme lateral variation in structure of the upper crust that exists in Iceland (Flovenz 1980).

SUMMARY AND DISCUSSION

The area for which we have determined crustal structures falls naturally into four subdivisions. The northern, Tertiary Trollaskagi block contains stations HOT12, HOT13, HOT27 and HOT14, the MVZ contains stations HOT26, HVE and SKR, the EVZ contains stations HOT23 and HOT25 and the southern region contains stations HOT21, HOT20 and HOT24. Our results are summarized in Fig. 17, which shows our best estimates for the depths to the bases of the upper and lower crusts.

Structures obtained for the Trollaskagi block vary in type from classical type 1 structures (e.g. station HOT13, southwest backazimuth) to type 2 structures (e.g. station HOT13, east backazimuth). Notwithstanding, the depth to the 6.5 km s^{-1} velocity horizon is consistent at ~8–9 km and to the 7.2 km s^{-1}

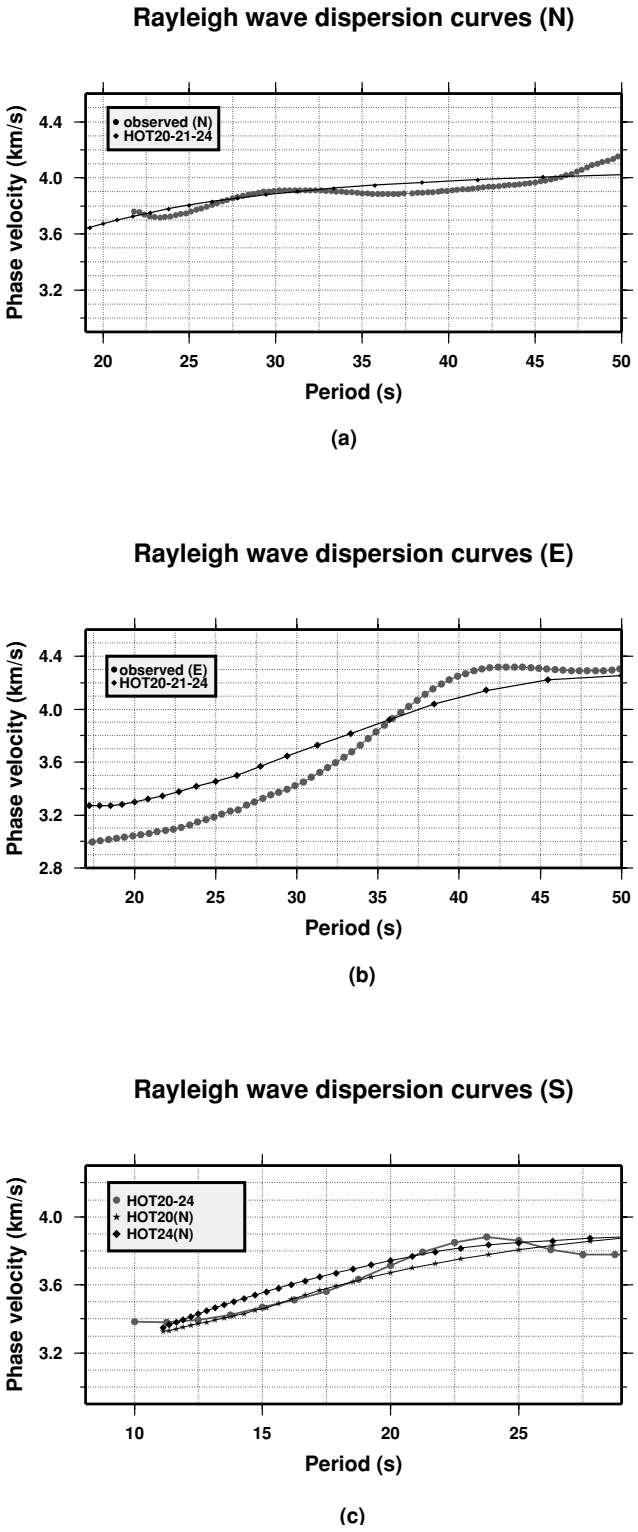

Figure 16. Same as Fig. 9 but for stations HOT21, HOT20 and HOT24 for (a) the north–south path HOT20–HOT24, (b) the east–west path HOT22–HOT21 and (c) the path between stations HOT20 and HOT24 compared with the predicted curves from the smoothest north backazimuthal models of stations HOT20 and HOT24.

horizon at 28–34 km. These provide a good definition for the bases of the upper and lower crusts respectively. Backazimuthal variations tend to be relatively small. Structures determined for the MVZ are unusual and do not fall into the spectrum between type 1 and type 2 structures. Very high velocities (exceeding 7 km s^{-1}) occur as shallow as 8 km depth, and as a result thicknesses for the upper crust defined by the 6.5 km s^{-1} horizon decrease to as little as $\sim$6 km beneath station SKR. A substantial LVZ occurs in the depth interval $\sim$20–35 km. Depths determined for the base of the lower crust are consistently in the range 35–40 km.

For stations within the EVZ and the NVZ, substantial backazimuthal variations occur. Our preferred estimates for the depths to the 6.5 and 7.2 km s^{-1} horizons, based on modelling of waveforms from a large local earthquake, are 5–8 and 35–38 km.

Structures beneath stations in the southern region show considerable lateral variation. The inversions using the north backazimuthal data yield a crustal discontinuity at a depth of $\sim$12 km, which defines the 6.5 km s^{-1} horizon beneath stations HOT21 and HOT20. This velocity discontinuity is well developed beneath stations HOT21 and HOT20 but unclear beneath station HOT24. Using the east backazimuthal data, depths obtained for the 6.5 km s^{-1} velocity horizon are $\sim$12 km beneath station HOT21 and $\sim$8 km beneath stations HOT20 and HOT24. The high velocity gradients characteristic of the upper crust give way to the low gradients characteristic of the lower crust consistently at depths of $\sim$4–5 km in the models from the north backazimuth data and at depths of 6–8 km in the models from the east backazimuth data. Our best estimates for the depth to the base of the upper crust under these stations are $\sim$5–6 km beneath station HOT21 and 4–8 km beneath stations HOT20 and HOT24 (Fig. 17). A clear demarcation of the lower crust and the crust–mantle transition is absent in this region, since a velocity discontinuity at the base of the lower crust is seen only in the structure obtained from the east backazimuthal data for station HOT24. The base of the lower crust, as defined by the 7.2 km s^{-1} velocity horizon, is at $\sim$25 km beneath station HOT21 and $\sim$30 km beneath stations HOT20 and HOT24.

In order to facilitate description and general interpretation, we have, in this paper, attempted the best summary possible for our results in the framework of the classical model of a bipartite crust underlain by a distinct crust–mantle interface or boundary zone. Using this approach, the following broad picture emerges. The thickness of the upper crust lies in the range 5–9 km and the depth to the base of the lower crust lies in the range 25–40 km. There is a tendency for the upper crust to thin and the lower crust to thicken beneath currently active rift zones and central volcanoes. This broad pattern is similar to that observed by Du & Foulger (1999) in their study of the Northwest Fjords area. There, the upper crust was seen to thin and the lower crust to thicken towards the nearest rift zone, which was, in that case, extinct. Such a trend is geologically reasonable. Kinematic modelling of lava eruption and spreading predicts that the lava pile that makes up much of the upper crust thickens away from the source rift zone (Palmason 1980). The partial melt and elevated temperatures at depths of some tens of kilometres beneath active rift zones and volcanoes would have the effect of lowering seismic velocities and depressing the depth to particular velocity horizons, e.g. the 7.2 km s^{-1} horizon. This would imply that, as the rift zones migrate laterally in Iceland, the depth to the base of the lower crust, if defined by seismic velocity, may migrate vertically. Furthermore, vigorous advection of melt upwards through the mantle would be expected to hinder the development of stable and

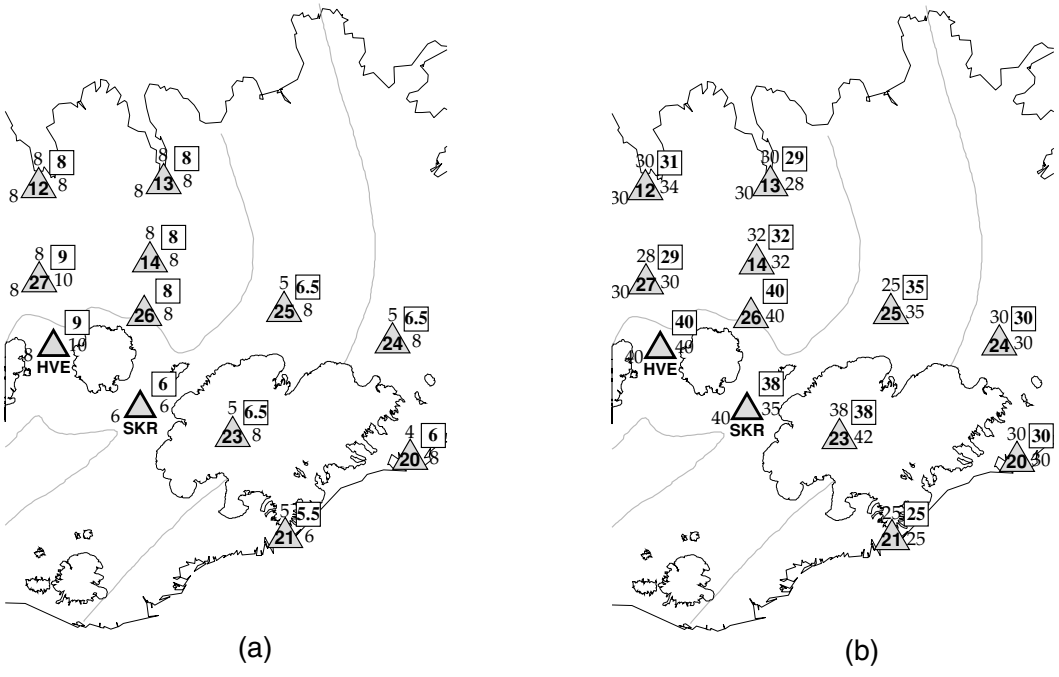

Figure 17. Maps of central Iceland showing the best estimates for depths to the bases of the upper and lower crusts. These are mostly taken to be the depths (a) at which V_p calculated from the results of the receiver functions reach 6.5 km s^{-1}, and (b) below which these values do not fall below 7.2 km s^{-1}. These are the average velocities found for the bases of the upper and lower crusts from refraction data throughout Iceland. In the cases of some results, these definitions were relaxed (see text for discussion). Triangles indicate the stations, and the numbers within indicate the station number. Unboxed integers: depths obtained from inverting the data from individual backazimuths. The positions of the digits around the stations indicate the backazimuth of the earthquakes used. Numbers in boxes: averages from all backazimuths, or best estimate from waveform modelling where there is considerable backazimuthal variation. The neovolcanic zones and glaciers are outlined.

distinct compositional or phase-based layering. This picture is supported by the observation that the thicknesses of the upper and lower crusts correlate to some extent with proximity to the most volcanically productive area.

Both the ICEMELT profile (Darbyshire *et al.* 1998) and the study described in this paper from multiple seismic data sources found that the upper crust thins over the currently active rift zone and that the crust–mantle boundary deepens from $\sim$30 to $\sim$40 km. The uncertainties in the depths to these horizons are estimated to be $\pm$0.6 and $\pm$2 km for the ICEMELT results and $\pm$1 and $\pm$2.5 km for the receiver function results. Differences in the depths determined to the bases of the upper and lower crusts are close to the combined uncertainties of the two methods. Considering that explosion seismic profiling samples the structure in a restricted, linear zone, whereas receiver functions and surface waves yield structures that are the average of a relatively large volume of crust around and beneath stations, the agreement is surprisingly good. The most substantial difference in the results is our finding of a substantial velocity inversion beneath the MVZ that is not modelled by Darbyshire *et al.* (1998, 2000). Such an inversion could result from a high-temperature gradient in the lower crust that depresses velocity with increasing depth at a greater rate than it is elevated by increasing pressure. This interpretation suggests that the lower-crustal temperature gradient beneath the MVZ is higher than beneath the EVZ and northwest Vatnajokull. This would suggest that the present centre of the hotspot, defined as the hottest region on a broad scale, may be more westerly than the culmination of shallow volcanism beneath northwest Vatnajokull, where it is generally assumed to lie. A possible explanation for why Darbyshire *et al.* (1998) did not detect the LVZ could be that it is more extreme in V_s (which is determined by receiver functions) than it is in V_p (which is determined by refraction profiling). A locally high V_p/V_s ratio of up to 2.0 might provide an explanation. Such a high V_p/V_s ratio would probably require the presence of partial melt, and it would be interesting to test this possibility independently.

A model of a simple Icelandic crust, everywhere clearly divided into upper and lower divisions and separated from the mantle by a sharp Moho is poorly supported by our results. The application of any consistent definition of the base of the upper crust, for example, the depth at which the velocity gradient radically decreases, the depth to the 6.5 km s^{-1} velocity horizon or the depth to a significant discontinuity, would yield large variations in the estimated thickness of the upper crust over Iceland. The same applies to definitions of the base of the lower crust. Furthermore, in the cases of structures of the second type, where a monotonic decrease in velocity gradient with depth characterizes the structure, the problem of dividing the structure into three distinct and contrasting elements on the basis of seismic velocity is ill-posed. Many of the structures we obtain for stations in Iceland are either of this type or deviate significantly in some way from being clear tripartite structures of the first type. We also find great variability in the nature of the interface between the crust and the mantle. There may be a major discontinuity (e.g. station HOT13, southwest backazimuth), a distinct zone several kilometres thick with enhanced velocity gradient (e.g. station HOT27, north backazimuth) or the absence of any distinct feature at all at reasonable depths (e.g. stations HOT21 and HOT20). The term 'Moho', originally used by Mohorovicic (1909) to define the boundary between the crust and mantle in Europe, is typically used

to mean a clear, sharp discontinuity of ~ 1.0 km s^{-1} in V_p. Under Iceland, in many places such a discontinuity is at best attenuated and laterally discontinuous.

ACKNOWLEDGMENTS

This research was funded by the Natural Environment Research Council (NERC) grants GST/02/1238 and GR3/10727. The data used were collected as part of the Iceland Hotspot Project, other participants of which were Richard Allen, Bergur H. Bergsson, Palmi Erlendsson, Steinunn Jakobsdottir, Bruce Julian, W. Jason Morgan, Guust Nolet, Matthew Pritchard, Sturla Ragnarsson, Ragnar Stefansson and Kristin Vogfjord. We thank NSF (grant EAR 9417918) and the IRIS/PASSCAL instrument center for technical assistance in deploying and running the seismic network. We acknowledge Bruce R. Julian and Lucy Bunce for useful discussions. The manuscript was improved by valuable reviews from two anonymous reviewers.

REFERENCES

Ammon, G.J., Randall, G.E. & Zandt, G., 1990. On the nonuniqueness of receiver functions, *J. geophys. Res.,* **95,** 15 303–15 318.

Bjarnason, I.Th., Menke, W., Flovenz, O.G. & Caress, D., 1993. Tomographic image of the mid-Atlantic plate boundary in southwestern Iceland, *J. geophys. Res.,* **98,** 6607–6622.

Darbyshire, F.A., Bjarnason, I.Th., White, R.S. & Flovenz, O.G., 1998. Crustal structure above the Iceland mantle plume imaged by the ICEMELT refraction profile, *Geophys. J. Int.,* **135,** 1131–1149.

Darbyshire, F.A., Priestley, K.F., White, R.S., Stefansson, R., Gudmundsson, G.B. & Jakobsdottir, S., 2000. Crustal structure of central and northern Iceland from analysis of teleseismic receiver functions, *Geophys. J. Int.,* **143,** 163–184.

Du, Z.J. & Foulger, G.R., 1999. The crustal structure beneath the Northwest Fjords, Iceland, from receiver functions and surface waves, *Geophys. J. Int.,* **139,** 419–432.

Foulger, G.R. & Toomey, D.R., 1989. Structure and evolution of the Hengill-Grensdalur central volcano complex, Iceland: geology, geophysics and seismic tomography, *J. geophys. Res.,* **94,** 17 511–17 522.

Flovenz, O., 1980. Seismic structure of the Icelandic crust above layer three and the relation between body wave velocity and the alteration of the basaltic crust, *J. Geophys.,* **47,** 211–220.

Gebrande, H., Miller, H. & Einarsson, P., 1980. Seismic structure of Iceland along the RRISP profile 1, *J. Geophys.,* **47,** 239–249.

Langston, C.A., 1979. Structure under Mount Rainier, Washington, inferred from teleseismic body waves, *J. geophys. Res.,* **84,** 4749–4762.

Levshin, A.L., Ratnikova, L. & Berger, J., 1992. Peculiarities of surface-wave propagation across central Eurasia, *Bull. seism. Soc. Am.,* **82,** 2464–2493.

Mangino, S., Priestley, K. & Ebel, J., 1999. The receiver structure beneath the China Digital Seismograph Network stations, *Bull. seism. Soc. Am.,* **89,** 1053–1076.

Menke, W., Brandsdottir, B., Einarsson, P. & Bjarnason, I.Th., 1996. Reinterpretation of the RRISP-77 Iceland shear-wave profiles, *Geophys. J. Int.,* **126,** 166–172.

Menke, W., West, M., Brandsdottir, B. & Sparks, D., 1998. Compressional and shear velocity structure of the lithosphere in northern Iceland, *Bull. seism. Soc. Am.,* **88,** 1561–1571.

Mohorovicic, A., 1909. Das Beben, *Jb. met. Obs. Zagreb (Agram.),* **9,** 1–63.

Nettles, M. & Ekstrom, G., 1998. Faulting mechanism of anomalous earthquakes near Bardarbunga volcano, Iceland, *J. geophys. Res.,* **103,** 17 973–17 983.

Ozalaybey, S., Savage, M.K., Sheehan, A.F., Louie, J.N. & Brune, J.N., 1997. Shear-wave velocity structure in the northern Basin and Range Province from the combined analysis of receiver functions and surface waves, *Bull. seism. Soc. Am.,* **87,** 183–199.

Palmason, G., 1980. A continuum model of crustal generation in Iceland; kinematic aspect, *J. Geophys.,* **47,** 7–18.

Panza, G.F., 1985. Synthetic seismograms: the Rayleigh waves modal summation, *J. Geophys.,* **58,** 125–145.

Saemundsson, K., 1979. Outline of the geology of Iceland, *Jokull,* **29,** 7–28.

Saemundsson, K., Kristjansson, L., McDougall, I. & Watkins, D.D., 1980. K-Ar dating, geological and palaeomagnetic study of a 5-km lava succession in northern Iceland, *J. geophys. Res.,* **85,** 3628–3646.

Staples, R.K., White, R.S., Brandsdottir, B., Menke, W., Maguire, P.K.H. & McBride, J.H., 1997. Faeroe-Iceland Ridge Experiment 1. Crustal structure of northeastern Iceland, *J. geophys. Res.,* **102,** 7849–7866.